DOE/ET-53088-336 IFSR #336*

Periodic Orbits for Reversible, Symplectic Mappings

Hyung-tae Kook and *James D. Meiss*
Institute for Fusion Studies
The University of Texas at Austin
Austin, Texas 78712

August 1988

***REVISED NOVEMBER 14, 1988**

Periodic Orbits for Reversible, Symplectic Mappings

Hyung-tae Kook and James D. Meiss
Institute for Fusion Studies
University of Texas
Austin TX 78712

August 5, 1988
revised Nov 14,1988

Abstract: A 2N dimensional symplectic mapping which satisfies the twist condition is obtained from a Lagrangian generating function $F(\mathbf{q},\mathbf{q}')$. The $\mathbf{q}$'s are assumed to be angle variables. Reversible maps of this form have 2^{N+1} invariant symmetry sets which are Lagrangian manifolds. We show that such maps have at least 2^N symmetric periodic orbits for each frequency $\omega=(m,n)$. Furthermore we show there is at least one orbit which minimizes the periodic action for each ω, and generically at least 2^N-1 other "minimax" orbits. There is "dominant" symmetry plane on which the minimizing orbit is never observed to occur. As a parameter varies, the symmetric orbits are observed to undergo symmetry breaking bifurcations, creating a pair of non-symmetric orbits. A pair of coupled standard maps provides a four dimensional example. For this case the two dimensional symmetry planes give a cross section of the resonances and a visualization of the Arnold web.

§1. Introduction

Sympléctic maps are useful for the description of many physical problems, including the motion of the asteroids,[1] particle accelerators,[2] plasma wave heating,[3] and the restricted three-body problem.[4,5] In particular any system described by a time independent Hamiltonian with N+1 degrees of freedom generates a 2N dimensional symplectic map by the Poincare surface of section.[3] Similarly an N degree of freedom, periodically time dependent Hamiltonian flow generates a symplectic map of the phase space by strobing at the forcing period.

A great deal is known about the periodic orbits of two-dimensional symplectic maps (area preserving maps). Poincare proposed, in his "last geometric theorem" that a map on the annulus which rotates the upper and lower boundaries of the annulus in opposite directions must have a fixed point. This was later proved by Birkhoff, and implies the existence of at least two periodic orbits for each period. For the case of twist maps on a cylinder, Mather and Aubry proved the existence of periodic orbits for any rotation frequency.[6,7] The mapping preserves the cyclic order of points on these orbits; this implies that a limit of frequencies approaching an irrational gives a quasiperiodic orbit.

The quasiperiodic orbits either densely cover invariant circles, or invariant Cantor sets. If the frequency is sufficiently irrational, the Kolmogorov-Arnold-Moser (KAM) theorem[4] guarantees the former occurs for small enough perturbations from the integrable case. The invariant Cantor sets, called cantori, are the remnants of the invariant circles after they have been destroyed. Knowledge of the properties of such orbits is extremely useful in understanding the break-up of invariant circles,[8] and the transport of orbits in the stochastic region of phase space.[9] In particular cantori are the dominant barriers for the flow of trajectories through phase space.

For higher dimensional mappings, much less is known. Recently, Bernstein and Katok[10] have shown that for C^1 perturbations from the integrable case there exist at least N+1 periodic orbits in a neighborhood of the unperturbed torus for any given commensurate frequency. However, the properties of incommensurate frequency

orbits are less clear. For many systems it can be shown that the KAM tori are destroyed for strong enough perturbations,[11] and it seems reasonable that, by analogy with the area preserving case, they will be replaced by remnant quasiperiodic orbits. In some cases these do exist and can be shown to be cantori;[12] however, whether this typically occurs and how the transition from the KAM regime occurs remain to be understood.

In this paper we consider symplectic maps with special properties: positive definite twist, and reversibility. In §2 we introduce our notation and the twist condition, which guarantees the existence of a Lagrangian type generating function. Positive definite twist is the analogue of the Legendre condition for continuous time systems. Orbital stability is discussed in §3, and in §4 we review the notion of reversibility: a system is reversible if each orbit is related to its time reverse by a symmetry transformation. Symmetric orbits must have points on N dimensional symmetry planes, and can be classified by which of these planes they intersect. This property is especially useful to reduce computational effort. An invariant torus must be invariant under the time reversal symmetry, and can be studied by considering nearby periodic orbits which are also symmetric.

Orbits of special interest occur at minima and minimax points of the action. For the area preserving case Aubry and Mather have shown the existence of global minima for each frequency. In our computations we easily find orbits which are locally minimizing for any rational frequency. Minimizing orbits are not always symmetric: we discuss symmetry breaking bifurcations in §5.

As an illustration we use a four dimensional generalization of the standard map due to Froeschle[13]. The configuration space is the two dimensional torus, and we use coordinates (q_1, q_2) with unit periods. The momenta are designated (p_1, p_2), and the map is given by

$$T: \begin{cases} p' = p - \nabla V(q) \\ q' = q + p' \end{cases} \qquad (1)$$

$$V(q_1,q_2) = \frac{-1}{(2\pi)^2}\left\{k_1\cos(2\pi q_1)+k_2\cos(2\pi q_2)+h\cos\left[2\pi(q_1+q_2)\right]\right\}$$

When only one of the three parameters (k_1,k_2,h) is non-zero this map has a global invariant: for example, if only h is non-zero then p_1-p_2 is conserved. If $h = 0$ then the map is separable into uncoupled two dimensional standard maps for (q_1,p_1) and (q_2,p_2). When h and at least one of k_1 or k_2 is non-zero it appears neither to have global invariants, nor to be separable.

For the four dimensional case, the symmetry planes are two dimensional, and thus in §6 we construct the orbital skeleton by plotting symmetric orbits which intersect a given symmetry plane. We find two distinct structures: resonances and channels. Corresponding to each periodic orbit with frequency $\omega = (m_1/n, m_2/n)$ is a resonance; its intersection with the symmetry plane is a two dimensional neighborhood in which there are no other rotational periodic orbits. Points initially in this region oscillate about the resonance for long periods. Corresponding to each commensurability, $\omega_1 j_1 + \omega_2 j_2 + j_3 = 0$, for integers j_1,j_2,j_3, we find a channel on the symmetry plane. These channels are the directions along which orbits "diffuse" by Arnold diffusion. Resonances occur at the intersection of an infinite number of channels. Outside the resonances and channels are closely packed periodic orbits, as well as the invariant tori or their remnants.

§2. Symplectic Twist Maps

Consider a dynamical system represented by a Lagrangian $L(\mathbf{q},\dot{\mathbf{q}},t)$. Here $\mathbf{q}$ is a point in some N-dimensional configuration space. The action of a path $\mathbf{q}(t)$, $t_0 \le t \le t_1$ is defined as

$$W[\mathbf{q}(t)] = \int_{t_0}^{t_1} L(\mathbf{q},\dot{\mathbf{q}},t)\,dt \tag{2}$$

Extremal paths, determined by setting the first variation, δW to zero for $\mathbf{q}(t_0)$ and $\mathbf{q}(t_1)$ fixed, satisfy the Euler-Lagrange equations of motion. If L is periodic in t with period one, then these equations can be formally converted into a mapping of the configuration space onto itself. A discrete Lagrangian can be defined by integrating L along an extremal orbit segment, $\mathbf{q}(t)$, which begins at the point $\mathbf{q}$ at t=0, and ends at $\mathbf{q}'$ at t=1

$$F(\mathbf{q},\mathbf{q}') \equiv \int_{\substack{0 \\ \mathbf{q}(t)\ \text{extremal}}}^{1} L(\mathbf{q},\dot{\mathbf{q}},t)\,dt \tag{3}$$

The action of an orbit segment from t=i to t=j can now be written

$$W(\mathbf{q}_i,\mathbf{q}_{i+1},\ldots\mathbf{q}_j) = \sum_{t=i}^{j-1} F(\mathbf{q}_t,\mathbf{q}_{t+1}) \tag{4}$$

Variation of W with respect to the intermediate points yields the mapping equations

$$\frac{\partial}{\partial \mathbf{q}_t}\left[F(\mathbf{q}_{t-1},\mathbf{q}_t) + F(\mathbf{q}_t,\mathbf{q}_{t+1})\right] = 0 \tag{5}$$

This equation locally defines a unique mapping, T, from $(\mathbf{q}_{t-1}, \mathbf{q}_t)$ to $(\mathbf{q}_t, \mathbf{q}_{t+1})$ providing $\det(\partial^2 F/\partial \mathbf{q}\partial \mathbf{q}')$ is never zero. We make a stronger assumption, the <u>twist condition</u>: the mixed partial derivative matrix is assumed to be uniformly negative definite, i.e. there exists a B>0 such that for any $\delta\mathbf{q}$, $\mathbf{q}$, $\mathbf{q}'$

$$\delta q \cdot b(q,q') \cdot \delta q \geq B \left| \delta q \right|^2$$

$$b(q,q') \equiv - \partial^2 F(q,q') / \partial q \partial q' \qquad (6)$$

It can be seen that this globally implies the existence of T.[11] The twist condition is the analogue of the Legendre condition in continuous time.

Equation (5) can be converted to Hamiltonian form by noting that F(q,q') can be taken to be a canonical generating function where the momenta are defined by

$$p' = \frac{\partial F(q,q')}{\partial q'} = F_2(q,q')$$

$$p = - \frac{\partial F(q,q')}{\partial q} = - F_1(q,q') \qquad (7)$$

where the subscripts F_1 and F_2 represent the partial derivatives of F with respect to its first and second arguments, respectively. These equations are implicit, but Eq. (6) implies they can be inverted to obtain an explicit mapping $z' = T(z)$ where $z \equiv (p,q)$ represents a phase space point. In phase space, the twist condition has a simple geometrical interpretation: an increment, δp, in momentum results in a position change in the same half space:

$$\delta p \cdot \delta q' \Big|_{\delta q = 0} > 0$$

A mapping is symplectic if it preserves the symplectic form ω, which is defined for two tangent vectors $\delta z = (\delta p, \delta q)$ and $\delta \tilde{z}$ as

$$\omega(\delta z, \delta \tilde{z}) = \delta z^i \, \omega_{ij} \, \delta \tilde{z}^j = \delta p \cdot \delta \tilde{q} - \delta q \cdot \delta \tilde{p} \qquad (8)$$

so that in canonical coordinates ω_{ij} is the matrix

$$\omega = \begin{bmatrix} 0 & I \\ -I & 0 \end{bmatrix} \qquad (9)$$

Thus if $(DT)^i{}_j = \partial z'^i / \partial z^j$ represents the Jacobian matrix, or tangent map; then T is symplectic providing

$$DT^t \omega DT = \omega \qquad (10)$$

where "t" designates transpose. If T is obtained from a canonical generating function, F, then it is automatically symplectic.

The symplectic form can also be expressed in terms of configuration space tangent vectors $(\delta q, \delta q')$, upon noting that $\delta p = -F_{11}\delta q - F_{12}\delta q'$:

$$\omega(\delta z, \delta \tilde{z}) = \delta \tilde{q} \cdot b \cdot \delta q' - \delta q \cdot b \cdot \delta \tilde{q}' \qquad (11)$$

where b is $b(q,q')$ defined by Eq. (6)

We will assume that the configuration variables represent physical angles with period one ($q + m \to q$, where m is an integer vector); thus the configuration space is the N-torus, $\mathcal{T}^N$, and the phase space is $\mathcal{R}^N \times \mathcal{T}^N$. This implies that the map commutes with translations by any integer vector m. Defining the translation operator R_m by

$$R_m q = q - m, \qquad (12)$$

then $TR_m = R_m T$. This implies that the generating function satisfies

$$F(q+m, q'+m) = F(q,q') + \mathcal{F}_m$$

where $\mathcal{F}_m$ is a constant. To interpret $\mathcal{F}_m$ let C be a curve in the phase space which connects (p,q) to $(p,q+m)$, and $C' = TC$ be its iterate. Parameterize these curves by $\lambda \in [0,1]$, so that $q(0)=q$, $q(1) = q+m$, etc. Using Eq. (7) we can show that the Poincare invariant between C' and C gives $\mathcal{F}_m$:

$$\int_{C'} p' \cdot dq' - \int_C p \cdot dq = \int_0^1 \frac{dF}{d\lambda}(q(\lambda), q'(\lambda))\, d\lambda = \mathcal{F}_m$$

or that $\mathcal{F}_m$ is the sum of the areas which move through the projections of the curve C onto the canonical planes; i.e. the net flux of symplectic area. The net flux clearly depends only on the homotopy class, m, of C; since there are N independent loops on $\mathcal{T}^N$ the net flux has N independent components. We will assume, as in example (1), that the net flux is zero.

An orbit is a doubly infinite sequence of configurations $\ldots q_t, q_{t+1}, q_{t+2}, \ldots$ such that every finite segment $\{q_t, q_{t+1}, \ldots q_s\}$ is a stationary point of the action $W(q_t, q_{t+1}, \ldots q_s)$ for given q_t and q_s. It is convenient to think of these orbits as occurring on the covering space of the N-torus, $\mathcal{R}^N$. Then the frequency (if it exists) is defined through a lift of the mapping as

$$\omega = \lim_{t-t' \to \infty} \frac{q(t) - q(t')}{t-t'} \tag{13}$$

(and is unique up to an integer vector).

An orbit is periodic with period n if

$$q_{t+n} = R_{-m} q_t \ , \quad p_{t+n} = p_t \tag{14}$$

for some integer vector m. Thus, every periodic orbit has a frequency $\omega = m/n$, which we also write as $\omega = (m,n)$. The action for a periodic orbit is

$$W_\omega(q_0, q_1, \ldots q_n) \equiv W(q_0, q_1, \ldots q_{n-1}, q_0+m) \tag{15}$$

Equation (15) gives a variational principle for periodic orbits: a periodic orbit of frequency ω is a critical point of W_ω where <u>all</u> points $q_0, q_1, \ldots q_{n-1}$ are varied freely. This is true because criticality of W_ω implies Eq.(5) for $0<t<n$, and variation with respect to q_0 implies $F_1(q_0, q_1) + F_2(q_{n-1}, q_0+m) = 0$, or by Eq.(7) $p_0 = p_n$.

An important class of symplectic maps are those with constant twist, i.e. $\mathbf{b}$ is a constant matrix. Such maps are of physical relevance because nonlinear maps typically have twist at least locally, and furthermore because an arbitrary twist map can locally be approximated by a map with constant twist. This is discussed extensively by Chirikov for the area preserving case.[14]

For the special case of constant twist, and zero net flux we show in Appendix A that the most general form for the generating function is

$$F = \frac{1}{2} (q' - q) \cdot \mathbf{b} \cdot (q' - q) \ - V(q) \tag{16}$$

where $\mathbf{b}$ is a symmetric matrix. The mapping generated by (16) is

$$T: \begin{cases} \mathbf{p}' = \mathbf{p} - \nabla V(\mathbf{q}) \\ \mathbf{q}' = \mathbf{q} + \mathbf{b}^{-1} \cdot \mathbf{p}' \end{cases} \qquad (17)$$

For N=1 the twist, $\mathbf{b}$, can be scaled to unity by a (non-canonical) change of coordinates; however, this cannot be done in general for N>1. The example (1) is of the form (17) with $\mathbf{b}$ chosen to be the identity matrix.

§3. Bifurcations and Loss of Stability

The stability of an orbit is determined by the tangent map $DT^n = \partial \mathbf{z}_n / \partial \mathbf{z}_0$, which is a symplectic matrix. As is well known,[4] if λ is an eigenvalue of a symplectic matrix then so are λ^{-1} and λ^*. This implies that the λ's come either in reciprocal pairs which are real or of modulus unity, or in a quadruplet with $\lambda_1 = \lambda_2^{-1} = \lambda_3^* = \lambda_4^{*-1}$. We will call the eigenvalues of DT^n the multipliers, to distinguish them from a later use of "eigenvalue". Let $\lambda_1, 1/\lambda_1, \ldots \lambda_N, 1/\lambda_N$ represent the complete set of multipliers and define the traces, ρ_i, and residues, R_i, as

$$\rho_i \equiv \lambda_i + 1/\lambda_i$$

$$R_i \equiv {}^1/_4(2 - \rho_i) \tag{18}$$

The orbit is stable only when all the traces are real and fall in the interval [-2,2], or equivalently the residues are real and in [0,1]. An orbit with a quadruplet of complex multipliers has a pair of complex conjugate residues; the residues are otherwise real.

In terms of the traces, characteristic polynomial is

$$\lambda^{-n} \det (DT^n - \lambda I) = \prod_{i=1}^{N} (\rho - \rho_i) = 0 \tag{19}$$

In general the coefficients of ρ^j, $j=0,1,\ldots, N-1$ in this polynomial give N parameters which determine the stability of the orbit. For N=2, the polynomial is quadratic

$$\rho^2 - A\rho + B - 2 = 0$$

$$A \equiv \mathrm{tr}(DT^n) = \rho_1 + \rho_2$$

$$B \equiv \frac{1}{2}\{[\mathrm{tr}(DT^n)]^2 - \mathrm{tr}[(DT^n)^2]\} = \rho_1 \rho_2 + 2 \tag{20}$$

Consequently, the two independent real quantities A and B determine the stability of the periodic orbit.[5] There are seven different regions

in the orbit stability diagram in the A-B plane, as shown in Fig. 1. The only stable region is the central area labelled "$\mathcal{EE}$"; it is bounded by the period-doubling bifurcation line (B=-2A-2), the saddle-node bifurcation line (B=2A-2) and the complex instability parabola ($B=A^2/4+2$). All the λ's have modulus one in the stable region, thus the orbit is doubly elliptic. The other stability regions are labelled using $\mathcal{E}$ for an elliptic multiplier pair, $\mathcal{H}$ for regular hyperbolic, $\mathcal{I}$ for inversion hyperbolic (a pair of negative multipliers). The final region, $\mathcal{CQ}$, corresponds to a complex quadruplet of multipliers. These seven regions can be mapped onto the parameter space for a given orbit, as shown in Fig. 2 for Eq. (1).

An alternative construction of the multipliers can be given in terms of the configuration space representation of the linearized mapping DT, which is obtained by linearizing Eq. (5):

$$-b_{t+1}\,\delta q_{t+1} + a_t\,\delta q_t - b_t^t\,\delta q_{t-1} = 0$$

$$b_t \equiv -F_{12}(q_{t-1}, q_t)$$

$$a_t \equiv F_{11}(q_t, q_{t+1}) + F_{22}(q_{t-1}, q_t) \qquad (21)$$

giving a linear second difference equation. The multipliers of a period n orbit are determined by the eigenvalue problem

$$\delta q_{t+n} = \lambda\,\delta q_t$$

which closes the recurrence relation (21). In matrix form, this can be rewritten as $\mathbf{M}\,\delta\mathbf{Q} = 0$ where $\delta\mathbf{Q} = (\delta q_0, \cdots, \delta q_{n-1})$ and the $(Nn)\times(Nn)$ dimensional matrix $\mathbf{M}(\lambda)$ is

$$M(\lambda) = \begin{pmatrix} a_0 & -b_1 & 0 & .. & \frac{-1}{\lambda} b_0^t \\ -b_1^t & a_1 & -b_2 & .. & 0 \\ 0 & .. & .. & .. & .. \\ .. & .. & .. & a_{n-2} & -b_{n-1} \\ -\lambda b_0 & .. & .. & -b_{n-1}^t & a_{n-1} \end{pmatrix} \tag{22}$$

Thus the multipliers are obtained by solving $\det M = 0$. This equation is an N^{th} order polynomial in λ and in $1/\lambda$; and since the mapping is symplectic we know this polynomial must be reflexive. Its roots are the multipliers, which are given by Eq. (19); thus it must have the form

$$\det M(\lambda) = C \prod_{i=1}^{N} (\rho_i - \rho)$$

where C is a constant independent of λ. In fact, C is precisely the coefficient of $(-\lambda)^N$ which is easily obtained from Eq. (22) by inspection, thus we obtain

$$\mathcal{M}(\lambda) \equiv \det M(\lambda) = \prod_{t=0}^{n-1} \det(b_t) \prod_{i=1}^{N} (\rho_i - \rho) \quad . \tag{23}$$

We will discuss these relationships further in §5.

When $\mathcal{M}(1) = 0$, the orbit has a pair of multipliers at +1. If, upon variation of parameters, a periodic orbit reaches a point where a multiplier is unity, then one of two things can happen. The orbit may collide with another orbit of the same period in which case the two orbits could be annihilated in a saddle-node bifurcation or they could pass through each other. Secondly, there may be a new pair of orbits created (or annihilated); this is the Rimmer bifurcation (see §4). It is commonly observed (i.e. co-dimension one) in the reversible case.

When $\mathcal{M}(-1) = 0$ the orbit has a pair of multipliers at -1. Upon variation of parameters such an orbit typically undergoes a period doubling bifurcation. These bifurcations have been studied for the four dimensional case by Mao and co-workers.[15]

The set $\mathcal{M}(\lambda) = 0$ for real p is a one parameter family of co-dimension one surfaces in the N dimensional stability parameter space. The envelope of this family, given by $\mathcal{M} = \mathcal{M}_p = 0$, is the co-dimension one complex instability surface, since these equations imply that $\mathcal{M}$ has a double root. For the four dimensional case this surface is the parabola $B=A^2/4+2$.

On one side of the complex instability surface there is a complex quadruplet of λ's. This boundary contains both the case of collision of two pairs of unit modulus multipliers (Krein collision), and of real multipliers (Fig. 3). Loss of stability by passing through this surface can occur only when the "Krein signature" of the two multiplier pairs on the unit circle is mixed.[16] Conversely, when the signature is definite, such a collision cannot lead to the complex instability: such an orbit is strongly stable under small perturbations. In the case of mixed signature, collision leading to the loss of stability typically occurs in one parameter families of maps, while for definite signature collisions are less common (co-dimension three).[17] However, for the case of the "in-phase" orbits of a coupled quadratic map, definite signature collisions without splitting off the unit circle naturally occur in the successive stable regions of the period doubling bifurcation sequence.[15]

For example (1), there are four fixed points, all at $\mathbf{p}=0$, and corresponding to $\mathbf{q} = m/2$. Stability is easily determined analytically. Figure 2(a) is the stability diagram when $k_2=0$ for the point $\mathbf{q}=0$. The stability diagrams for the other three points are obtained from this by flipping the signs of k_1 and/or h:

q	(0,0)	$(0,\frac{1}{2})$	$(\frac{1}{2},0)$	$(\frac{1}{2},\frac{1}{2})$
signs	(k_1,h)	$(k_1,-h)$	$(-k_1,-h)$	$(-k_1,h)$

The stable region is labelled $\mathcal{EE}$. For any given parameters only one fixed point can be $\mathcal{EE}$; when k_1 and h are positive, this is the point $\mathbf{q}=(0,0)$. In this case the point $(\frac{1}{2}, 0)$ is always hyperbolic. The other

two fixed points have one hyperbolic direction (negative residue) and one direction which is either elliptic or inversion hyperbolic (positive residue). Complex instability does not occur since the signature of the stable region is definite.

There are also four period two orbits with frequency (1,1,2). The stability of the period two orbits can be analytically determined for the two orbits at $\mathbf{q} = (0,0) \rightarrow (1/2, 1/2)$ and at $(1/2, 0) \rightarrow (0, 1/2)$. The diagram for the first orbit is Figure (2b); for the second reverse the signs of both k_1 and h. In region $\mathcal{EE}_1$ the multipliers have definite signatures, and there are no collisions except at $\lambda = \pm 1$, hence there is no complex instability boundary. However there are two more stable regions for the period 2 case (region $\mathcal{EE}_2$ and $\mathcal{EE}_3$ of (b)) for which the signatures are mixed, and for which there is a boundary leading to region $\mathcal{CQ}$. Note that a bifurcation to $\mathcal{CQ}$ can not only occur from an $\mathcal{EE}$ region, as sketched in Fig. (3a), but also from $\mathcal{HH}$, as in Fig. (3b), or $\mathcal{II}$.

In numerical computations for higher periods, we commonly observe (upon the variation of a single parameter) the collision of two multiplier pairs either on the unit circle or the real axis leading to the $\mathcal{CQ}$ region. We will discuss this further below.

§4. Reversibility

The flow generated by the simple Hamiltonian $H = {}^1/_2 p^2 + V(q)$ is time reversible; for every orbit $[p(t),q(t)]$ there is another orbit $[-p(-t),q(-t)]$, which is its time reverse. Time reversal is accomplished by reversing the momentum. In general a map is <u>reversible</u> if there is an anti-symplectic involution, S, which reverses time:[18,19]

$$STS = T^{-1} \tag{24}$$

S is anti-symplectic if $DS^t\omega DS = -\omega$, and an involution if $S^2 = I$. Equation (24) implies that the map can be factored as

$$T = (TS)S$$

showing that TS is also an anti-symplectic involution. Since it satisfies (24), it is also also a reversor for T, called the <u>complementary symmetry</u> to S. In fact, each operator T^kS is also a symmetry of T, with complementary symmetry $T^{k+1}S$.

A set invariant under the symmetry operator is called a symmetry set. Near a fixed point of S, symplectic coordinates (ξ,η) can always be found such that $S(\xi,\eta) = (-\xi,\eta)$.[20] Thus the symmetry sets are N-dimensional submanifolds, which we will call <u>symmetry planes</u>. In fact they are Lagrangian manifolds, since if δz and $\delta\tilde{z}$ are tangent vectors at a point z_0 in Fix(S), then $\delta z = DS\delta z$, and therefore $\delta z^tDS^t\omega DS\delta\tilde{z} = \delta z^t\omega\delta\tilde{z}$; the anti-symplectic condition implies this is equal to its negative and therefore $\delta z^t\omega\delta\tilde{z} = 0$. We will assume that these manifolds are graphs over the momentum plane.

As an example, the map generated by eq. (16) is easily shown to be reversible if $V(q) = V(-q)$; a pair of symmetry operators is

$$S: \begin{cases} p' = p - \nabla V(q) \\ q' = -q \end{cases}$$

$$TS: \begin{cases} p' = p \\ q' = -q + b^{-1}\cdot p \end{cases} \tag{25}$$

The fixed sets of these symmetries are the N-planes, Fix(S) = {**q** = **0**}, and Fix(TS) = {**p** = 2**b**·**q**}. This applies to the Froeshle example (1).

Due to the periodicity of T, there are other symmetries obtained from the above by translation: the translation of a symmetry by an integer vector **m**, the operator $SR_{\mathbf{m}}$, is also a symmetry. It is easy to see that upon translation the fixed sets are translated by half integral vectors; for the example (25) this gives

$$\mathrm{Fix}(SR_{\mathbf{m}}) = \{\mathbf{p},\mathbf{q} \mid \mathbf{q} = {}^1/_2\mathbf{m}\}$$

$$\mathrm{Fix}(TSR_{\mathbf{m}}) = \{\mathbf{p},\mathbf{q} \mid \mathbf{p} = 2\mathbf{b}\cdot(\mathbf{q} - {}^1/_2\mathbf{m})\} \qquad (26)$$

These fixed sets are indeed Lagrangian manifolds since **b** is symmetric.

On the torus, there are 2^N symmetry planes for S, obtained by letting the elements of **m** be either 0 or 1, and the same number generated by TS. Of course each symmetry family $(T^jS, T^{j+1}S)$ has such a set of symmetry planes.

Symmetric orbits are those invariant with respect to time reversal, which means that for the symmetry S and an orbit $\{\mathbf{z}_t\}$ each point $\mathbf{z}_i$ has a symmetric counterpart: there exists a j such that $\mathbf{z}_j = S\mathbf{z}_i$.

The importance of symmetric orbits arises from three facts. Firstly, it is easy to see that every symmetric orbit must have a point on a symmetry plane.[19] If $\mathbf{z}_j = S\mathbf{z}_i$ and k = j-i is even, then Eq. (24) implies

$$\mathbf{z}_{i+k/2} = T^{-k/2}\mathbf{z}_j = T^{-k/2}S\mathbf{z}_i = ST^{k/2}\mathbf{z}_i$$

or that $\mathbf{z}_{i+k/2}$ is a fixed point of S. On the other hand if k is odd then $\mathbf{z}_{i+(k+1)/2}$ is a fixed point of TS. This greatly simplifies finding symmetric orbits by limiting the search to the symmetry planes.

Secondly, each symmetric periodic orbit of frequency (**m**,n) has a second point on another symmetry plane. Suppose $\mathbf{z}_i$ is a fixed point of some symmetry, S'. Eq. (24) implies

$$\mathbf{z}_{i+j} = S'\mathbf{z}_{i-j} \qquad (27)$$

Applying the periodicity condition, Eq. (14), to this yields

$$z_{i+j} = R_{-m}\, T^{-n} S' z_{i-j} = R_{-m}\, S' z_{n+i-j}$$

$$= S' R_m\, z_{n+i-j} \qquad (28)$$

Now pick $j = k \equiv [(n+1)/2]$, where [] represents integer part. Equation (28) implies that z_{i+k} is a fixed point of $S'R_m$ for n even and of $TS'R_m$ for n odd.

Conversely, suppose we have an orbit segment $\{z_0, z_1, \ldots z_k\}$ such that $z_0 \in \mathrm{Fix}(S')$, and $z_k \in \mathrm{Fix}(S'R_m)$ for some symmetry S'. A periodic orbit of period $n=2k$ is obtained by using Eq. (28) with $i=0$ to define the z_j for $j \in [k+1, n]$. This implies that $z_n = S'R_m z_0 = R_{-m}\, z_0$, so that the orbit is indeed periodic and has frequency (m, n). A similar construction applies to the odd period case, for which $z_k \in \mathrm{Fix}(TS'R_m)$, and $n = 2k+1$. Thus a symmetric orbit of period n can be obtained by searching for a segment of length k which has end points on two symmetry planes (see Appendix C).

The final reason for the studying symmetric orbits is that every invariant torus which is homotopic to $p=0$ and which has a dense orbit, must be symmetric, since it must intersect the symmetry planes. Thus it seems reasonable to use symmetric periodic orbits to approximate quasiperiodic orbits.

Classification of the symmetric orbits is attained by considering the the phase space $\mathcal{R}^N \times \mathcal{T}^N$ where there are 2^{N+1} distinct symmetry planes generated by S and TS. Each symmetric orbit as a point on two of these planes, and so there are 2^N types (with one exception, see below). Using the above relation, the classes can be easily obtained for each (m,n); they depend only on the evenness or oddness of the components of the frequency. In table 1 the classification is given for N=2 where there are eight frequency types. For example when the frequency is of the type (even,odd,odd), then the symmetric orbit with a point on the Fix(S) plane, also has a point on the $\mathrm{Fix}(TSR_{(0,1)})$ plane. These two symmetric points are indicated by open circles on each canonical plane in Fig. 4. The other three symmetric orbits are also shown in the figure. The case (even,even,even) in Table 1 refers to an orbit which has a minimal period which is even, and yet the elements of m are also even; such orbits arise, for example, from period doubling bifurcations.

In Appendix B we show that there will be at least one orbit of each symmetry class for each frequency. Therefore a reversible, symplectic twist map has at least 2^N symmetric periodic orbits for each frequency (m,n).

For the four dimensional example (1) we routinely find all four symmetric periodic orbits for any given frequency. The simplest technique is to begin with a point in the first symmetry plane in Table 1 and vary p until the orbit returns to the second symmetry plane in Table 1 after k iterations. This requires a 2D root finding routine; we use Broyden's method (see Appendix C), which is a generalization of the secant method. This method fails to converge when the parameters (k_1,k_2,h) are large because the orbits are strongly unstable, but reasonably large parameters can be obtained by using extrapolation from small parameter values to give good initial guesses.

A more sophisticated technique is based on Newton's method for extremizing the action W_ω. We use this method when the orbits are strongly unstable; however, it also requires good initial guesses. The details of this method will be discussed in a future paper.

Figure 5 displays a projection of the four symmetric orbits of frequency (12,21,49) onto the q-plane. Note that, except for the point at $q = (0,0)$, the orbits tend to avoid the region near the origin. This phenomena will be be explained in terms of the action function in the next section.

Typically, when the parameters (k_1,k_2,h) are not too large, one of the symmetric orbits is of type $\mathcal{EE}$, another is $\mathcal{HH}$, and the remaining two are $\mathcal{EH}$ (we observed this already for period one and two in §3). This is the analogue of the familiar island chain formed by an elliptic-hyperbolic pair for the area preserving map. As the parameters increase various bifurcations can occur as shown in Fig. 6. For example in Fig. 6(a), the (2,3,4) orbit on Fix(S) first undergoes a period doubling bifurcation, then regains stability by its inverse (thus the period eight orbit only exists for a limited range, forming a "bubble"), only to loose it again by a complex bifurcation. The multipliers coalesce on the real axis in an inverse Krein collision. The resulting $\mathcal{HH}$ orbit then undergoes a symmetry breaking bifurcation to $\mathcal{EH}$ when a pair of multipliers passes through $+1$.[21] When this occurs a pair of non-symmetric orbits with the the same period is created, as

shown in Fig. 7(b), and the residue corresponding to the original orbit changes sign. There is a corresponding change in sign of $\mathcal{M}(1)$. Finally the orbit reaches the $\mathcal{H}$ region. Similarly the orbit on $\mathrm{Fix}(SR_{(1,0)})$ undergoes the normal symmetry breaking bifurcation shown in Fig. 7(a). Spiraling in the A-B plane like that shown in Fig. 6 is common, and becomes more rapid for longer period orbits.

Symmetry breaking bifurcations of the ordered periodic orbits do not appear to occur for the standard map (the minimizing orbit always appears to be symmetric), but can occur for a more generally, for example, when the potential is $V(q) = a_1\cos(2\pi q) + a_2\cos(4\pi q)$ and a_2 is large enough.

§5 Minimizing Orbits

For area preserving twist maps, existence theorems for periodic and quasiperiodic orbits are based to a large extent on the properties of the action. Aubry and Mather prove, for example, that an area preserving twist map has a minimizing orbit for each (m,n).[6,7] An orbit is defined to be minimizing if the action of every finite segment of the orbit is not larger than that of any variation with fixed end points:

$$W(q_j,\ldots,q_k) \leq W(q_j, q_{j+1}+\Delta q_{j+1}, \ldots q_{k-1}+\Delta q_{k-1}, q_k)$$

for all j<k. Aubry shows that an (m,n) minimizing configuration is ordered on the circle in the same way as a simple rotation with frequency m/n. This implies that there also exists a second periodic orbit of frequency (m,n) because if the the orbit of q_0 is minimizing, then so is that of $T^t q_0$. If we choose t so that $T^t q_0$ is the nearest point on the orbit to the right of q_0, then between these neighbors there occurs a point which is minimum in all directions except one; this is the minimax configuration.

For N>1 the straightforward generalization of Aubry's minimizing condition does not appear to be fruitful. We use a weaker definition: a periodic orbit $\{q_t\}$ is a <u>minimizing</u> if its periodic action (15) is not larger than any other periodic configuration

$$W_\omega(q_t) \leq W_\omega(q_t + \Delta q_t) \qquad (29)$$

This does not in general imply that the orbit is minimizing in Aubry's sense: a counter-example is given by Hedlund for geodesics on a three torus.[22] He shows that a geodesic of given winding number ω which minimizes the analogue of W_ω, may not be a minimum of the periodic action for some multiple of the winding number: $W_{j\omega}$. In this case minimizing orbits (in Aubry's sense) do not exist for each ω.

A periodic orbit is <u>locally minimizing</u> if the second variation of the periodic action about the orbit is positive definite. This latter concept is all that we can check numerically.

The <u>Morse index</u> of the action is defined as the number of convex directions at its extremum, i.e. the number of the negative

eigenvalues of the quadratic form $\delta^2 W_\omega$.[23] A minimizing orbit has index zero.

In Appendix B we show that there exist minimizing periodic orbits for each frequency. This result follows from a bound on the growth of the generating function with $|q - q'|$ entirely analogous to the area preserving case. Furthermore, there exist orbits with non-zero indices as well (Appendix B). The minimum of the periodic action for a given value of q_0 exists, and gives a function on the N-torus. Each critical point of this function gives a periodic oribit. Generically the critical points of such a function are non-degenerate, and in this case Morse theory implies that there are at least 2^N. Thus there are typically at least 2^N orbits for each frequency (m,n). The indices of these orbits range from 0 to N, and there will typically be at least N!/i!(N-i)! orbits with index i.

There is a close relationship between the stability matrix (22) and the second variation of the action (15) about the periodic orbit:

$$\delta^2 W_\omega\Big|_{\delta Q} = \frac{1}{2}\delta Q^t M(1)\delta Q \tag{30}$$

where δQ represents an arbitrary variation. Thus M(1) is the Hessian matrix corresponding to the quadratic form $\delta^2 W_\omega$. For the area preserving case the stability type of a periodic orbit is characterized solely by the determinant of M(1),[24] however when N>1, this is no longer true. We can combine (23) and (30) to obtain a relation which generalizes the area preserving case:

$$\prod_{i=1}^{N} R_i = \left(-\frac{1}{4}\right)^N \frac{\mathcal{M}(1)}{\prod_t \det b_t} \tag{31}$$

where the R_i are the residues (18). Since b is assumed positive definite, Eq. (31) gives a relationship between the sign of the product of the residues, and of the determinant of the second variation of the action:

> If the index is odd (even) then there must be an odd (even) number of residues which are real and positive.

For the area preserving case, a non-degenerate minimizing orbit must be regular hyperbolic. For four dimensions a minimizing orbit falls in the region B>2A-2, i.e. above the saddle node line in Fig. 1; this does not completely determine its stability type, excluding only the cases $\mathcal{EH}$ and $\mathcal{HI}$.

We often find that as the parameters (k_1,k_2,h) are increased from zero one of the symmetric orbits is minimizing and of type $\mathcal{HH}$. This orbit can undergo a symmetry breaking bifurcation, however, and its index will become one. The action as a function of a configuration variable will undergo an evolution like that shown in Fig. 8. The two newly created non-symmetric orbits are now minimizing, and of type $\mathcal{HH}$, as indicated in Fig. 7(b). Similarly, the non-zero index, symmetric orbits can also spawn non-symmetric orbits.

The symmetry plane which goes through the maximum of $F(\mathbf{q},\mathbf{q})$ plays a special role, and we will call this plane the dominant symmetry plane.[19] In particular the index N fixed point occurs on the dominant symmetry plane. Furthermore F has critical points on each of the other symmetry planes $\mathrm{Fix}(SR_m)$, and so there are fixed points on each. In general there may also be other critical points of F, which give non-symmetric fixed points.

Now consider periodic orbits of other frequencies $\boldsymbol{\omega}$. For large enough potential $V(\mathbf{q})$, a minimizing orbit should have most of its points near the minimum of -V, since the potential dominates the action, Eq. (16). An orbit with dominant symmetry, however, must have a point on the plane where -V is maximum, and thus ought to have an action larger than those without points on this plane. It certainly seems reasonable that the minimizing orbit will not have a point on the dominant symmetry plane, and we conjecture that the minimizing orbit never has the dominant symmetry. For the case N=1 this conjecture is supported by extensive numerical evidence.[9,19]

Our scans of parameter space for the example (1) have never given a minimizing orbit on the dominant plane. For most cases the index two orbit has the dominant symmetry for small parameter values; however, as the parameters increase the orbit on the dominant plane can undergo a symmetry breaking bifurcation, and then will no longer have index 2. We also see, as in Fig. 5, that the minimizing and index one orbits tend to avoid the dominant plane, leaving a hole inside of which sits a single point of the index two orbit. As the

parameters are increased this hole grows in size until it encircles the torus producing a stripe which is seen in Fig. 5. We suspect that a similar phenomena for quasiperiodic orbits is responsible for the destruction of an invariant torus.

§6. Simultaneous Rational Approximations and Resonances

In this last section, before discussing the structure of phase space in terms of resonances and stochastic layers, we briefly review some results of the theory for the simultaneous approximation of sets of irrationals by rationals.

In studies of dynamical systems, many results from number theory have been used, sometimes in the proof of theorems, but also for the purpose of practical calculations. For example, the observation that an irrational number can be far from rationals (theorem 23 in Khinchin[25]) was one of the key ideas in the proof of the KAM theorem[4] which asserts that most non-resonant irrational tori survive for nearly integrable systems.

The continued fraction algorithm is one of most frequently used tools in the study of area preserving mappings.[25] It is a scheme for systematically generating a sequence of rational approximations, m_i/n_i to a number ω. It has many important properties of which we mention three. Firstly, it is strongly convergent (i.e. for any ε $\exists$ j such that the norm $|m_i-\omega n_i| < \varepsilon$ $\forall$ $i \geq j$. Weak convergence uses the norm $|\omega-m_i/n_i|$). Secondly, all the rational approximants to an irrational number are best approximants in the strong sense (given an approximant m/n to ω, there are no m'/n' with n'<n satisfying $|m'-\omega n'| < |m-\omega n|$).[25,26] Another merit of the algorithm is that the quadratic numbers (roots of a 2^{nd} degree monic polynomial) are characterized by the periodicity of their continued fraction (Lagrange's theorem).

For the higher dimensional case, one would like to approximate a vector $\boldsymbol{\omega}$ by a set of rationals with common denominator, $\mathbf{m}/n$. For the case N=2, such a continued fraction algorithm was first given by Jacobi (1868). His idea has been extended for general N by Perron (1907) and the algorithm is known as the "Jacobi-Perron" algorithm.[27] It is weakly convergent for all N; however, it does not generate all the best approximants. Furthermore, the characterization of numbers for which the Jacobi-Perron algorithm is periodic is unknown.

Many other algorithms have been devised to approximate irrationals with simultaneous n-tuple rationals. Among these, the work of Brentjes may be valuable for application to dynamical systems.[28] His algorithm produces all the best rational approximants

for N=2. However the sequence of approximants also contains other rationals besides the best and, consequently converges more slowly than optimal. The implementation of this algorithm on the computer is straightforward except that one must do inordinately long calculations to determine the direction of successive approximation at each level. No algorithm has yet been shown to be suited for the characterization of numbers analogous to Lagrange's theorem.

The Farey tree[29] is well known as an alternative scheme for approximating irrational numbers; it is strongly converging for irrationals, and gives all the best approximants. Even though it converges more slowly than the continued fraction, it is often more valuable due to its elegance in organizing the real numbers. The tree generates all rational numbers together with the irrationals as limits of paths, and every number is associated with a unique path. Furthermore this path provides a binary coding for the reals.

Recently, this algorithm has been successfully extended to the N=2 case by Kim and Ostlund.[26] Even though it does not generally produce the sequence of best approximants, it presents a very elegant way of organizing simultaneous rationals. The tree is obtained from a set of three integers vectors $(\mathbf{a}, \mathbf{b}, \mathbf{c})$ in $\mathcal{R}^3$, which satisfy $\mathbf{a}\cdot\mathbf{b}\times\mathbf{c} = 1$, for example (1,0,1), (0,1,1), and (0,0,1). Each vector represents a pair of rationals with common denominator, $\mathbf{a} \rightarrow (a_1/a_3, a_2/a_3)$. The vectors can be represented symbolically as the vertices of a right isosceles triangle, as shown in Fig. 9. The level zero rational is obtained by vector (Farey) sum of the hypotenuse vertices: $\mathbf{a}+\mathbf{b} = (a_1+b_1, a_2+b_2, a_3+b_3)$, and is represented by the midpoint of the hypotenuse. The original triangle is now divided into two right isosceles triangles, each of which can be used to construct a new vertex on level one, giving four triangles for the next level. The vertices of each Farey triangle satisfy $\mathbf{a}\cdot\mathbf{b}\times\mathbf{c} = 1$ by construction. One can show that every rational pair (in the convex hull of $(\mathbf{a},\mathbf{b},\mathbf{c})$) is obtained by a finite path on the tree; however, every one inside the triangle $(\mathbf{a},\mathbf{b},\mathbf{c})$ is obtained by two paths. This multiplicity is inconvenient, but not crucial in the manipulation of the algorithm. Furthermore every rational pair is in lowest common terms. It has been also shown that the numbers can be addressed by binary codes so that the algorithm can be handled with the shift operation on the

corresponding address. This coding scheme makes the computational implementation of the algorithm very convenient.

The symmetry and the self-similar structure inherited from the binary construction is shown in Fig. 10 which displays the rationals $\omega=(\omega_1,\omega_2)$ in the range $[-1/2,1/2] \times [-1/2,1/2]$ produced by the generalized Farey tree algorithm up to level 13. On the ω plane each triangle is not actually right isosceles; for example, one of the level two triangles has vertices $(0/1,0/1)$, $(1/2,0/2)$ and $(1/3,1/3)$. Notice that the sampling is extremely non-uniform, with sparse regions around every rational pair. These of course will be densely filled by higher level rationals, and in the limit of infinite level, by incommensurate pairs.

Our numerical results suggest the close contact of the generalized Farey tree construction to the dynamics of four dimensional mappings. The points in Fig. 10 are equivalent to the intersections of periodic orbits of the frequency ω on a constant angle plane for the integrable map: for example (1) with $k_1= k_2= h= 0$, a periodic orbit with frequency ω occurs at $p=\omega$. This symmetry is broken as soon as the parameters are non-zero, as shown in Fig. 11 for the same set of periodic orbits. The orbits are obtained by using Broyden's method (discussed in Appendix C), and are all symmetric since they are either (a) on the Fix(S) plane or (b) on the $\mathrm{Fix}(SR_{(1,1)})$ plane. Now the sparse regions are larger, and are not filled in by higher level orbits.

The structure is analogous to that for area preserving maps. Figure 11(a) corresponds to the dominant symmetry line of the standard map. Every ordered minimax orbit of the standard map seems to have a point on this line, and each corresponds to the center of a resonance.[31] There are no other ordered orbits for some interval around minimax periodic orbit. These intervals are bounded by the minimax orbits which are homoclinic to the minimizing orbit of the resonance. Sequences of symmetric periodic orbits which limit to a rational, for example the sequences $\pm 1/n$, limit to homoclinic orbits as $n \to \infty$, and not to the minimax periodic orbit. In the full two dimensional phase space, we define a resonance as an area bounded by segments of the stable an unstable manifolds of the minimizing orbit. Thus the structure on the symmetry line reflects this partition of

phase space. If there are rotational invariant tori, they must exist outside the vacant intervals on the symmetry line.

For the four dimensional mapping, higher period orbits also tend to be expelled from the vicinity of shorter periodic orbits on the symmetry plane to form resonance zones around each periodic orbit. Orbits in the resonance zone tend to remain trapped in the zone for long periods. The resonances occupy four dimensional volumes, which cut the symmetry plane in two dimensional regions. In Fig. 11, we associate the empty region surrounding the (0,0,1) orbit, with the (0,0,1) resonance. Many other such region are visible in the figure. The boundaries of the resonances, which should be three dimensional, are not easy to define; they do not consist solely of stable and unstable manifolds of the $\mathcal{HH}$ orbit, since these are merely two dimensional, but appears to include many other orbits, as we will discuss below.

There appear to be channels which connect the resonances, each corresponds to a commensurability relation, $\omega_1 j_1 + \omega_2 j_2 + j_3 = 0$, or equivalently $\omega \cdot j = 0$ for the representation $\omega = (m_1, m_2, n)$. For example the horizontal and vertical channels corresponding to $j = (0,1,0)$ and $(1,0,0)$ have widths controlled by the parameters k_2 and k_1, respectively. Similarly, the major diagonal channel, with $j = (1,1,0)$, corresponds to the coupling term, h, in Eq. (1). Other channels are generated by higher order commensurabilities, and their widths could be obtained from perturbation theory.[14] Along the channels there are an infinity of resonances which satisfy the commensurability relation; in fact, as we will see below the channels seem to be composed of these resonances.

Orbits initially in a resonance zone may eventually leave the zone, even if they are started arbitrarily close to the central $\mathcal{EE}$ orbit: this is the process called Arnold diffusion.[3,14] Similarly an orbit in the chaotic region outside a resonance can wander into resonances since invariant tori do not separate the phase space. The transitions from resonance to resonance occur along the commensurability channels, which form the so called Arnold web. However central portions of the resonances are difficult to enter.

This is shown in Fig. 12, which is a thin slice of the phase space near the dominant symmetry plane. Two initial conditions were iterated for 2×10^8 iterations, and only those points which fall in the slice are plotted (an equivalent figure is given in Ref. 30). Many of the

resonance zones shown in Fig. 11 are inaccessible on this time scale. The inaccessible regions appear to have fairly sharp, but irregular boundaries. On these there are many sticky points, corresponding to dark spots on the figure: these points correspond to invariant tori trapped in the resonance. Figure 13 shows one such torus in the primary resonance. There are many irrational tori around each resonance; however, they do not form a complete barrier: transition into a resonance occurs through the gaps between tori.

To attempt to delineate the resonance boundaries more precisely we could consider the homoclinic orbits. However, there appear to be only a few (perhaps four) homoclinic orbits on the dominant symmetry plane. For the (0,0,1) resonance these correspond, to the limits of the sequences (m_1,m_2,n) with $m_i=\pm 1$ and $n\to\infty$. In Fig. 11 these sequences are visible as the traces down the middle of the diagonal channels. Other sequences of periodic orbits, for example those in the vertical and horizontal channels given by $(0,\pm 1,n)$ or $(\pm 1,0,n)$, seem to limit to these four primary homoclinic orbits, or sums of these orbits.

A frequency analysis can also be used to find the resonance boundaries. All orbits trapped forever inside a resonance will have the same frequency, Eq. (13), as the resonance. So we can approximately delineate the resonance region by computing the frequency for some finite period of time; let ρ be this finite time frequency. Since, as Fig. 12 shows, Arnold diffusion is quite slow from the resonances, we can expect to obtain reasonable results even for modestly long times; we choose a time interval so that it would be shorter than an Arnold diffusion time scale but long enough to give statistical average. Typically we use $t=10^3$ with the parameter values we present. Figure 14 shows ρ_1 calculated for a set of initial conditions on the line $p_1=-p_2$ and $q_1=q_2=0$. A similar figure is obtained for ρ_2, except with negative slope. These initial conditions lie in the diagonal channel corresponding to $j=(1,1,0)$ which is seen in Figs. 11(a) and 12. There are flat steps in $\rho(p)$ corresponding to resonances of the form $(m,-m,n)$ showing that the channel is actually a collection of many resonances stacked closely together. The scattering of points near the edges of each resonance correspond to highly stochastic orbits.

Similarly, Fig.15 shows regions which have frequencies corresponding to low order resonances; it is a complementary view to that in Fig.12. To construct Fig. 15 we consider initial conditions on a grid on the $q=0$ plane. Each is iterated 10^3 times, and points are filled in only if $|\rho(p) - \omega| < \varepsilon$ for ω on the generalized Farey tree up to level five. The size of each resonance area on this plane depends weakly on the time scale we use to define the rotation number, but they correspond closely to the avoided regions in Fig. 12. The boundary of a resonance is not smooth, due to the stochastic orbits near its edge. The closer to the boundary an orbit is, the faster it escapes out of the resonance.

§7 Conclusions

We have shown that reversible, symplectic, twist mappings of a 2N dimensional phase space have periodic orbits which can be classified by frequency, symmetry, and Morse index. Such mappings have 2^N different types of symmetric orbits for each rational frequency vector ω. For each frequency we also find 2^N orbits for which the action function has indices ranging from 0 to N. For small deviations from the trivial twist map ($k_1=k_2=h=0$) these two sets of orbits often coincide; however the symmetric orbits commonly undergo symmetry breaking bifurcations which change their indices.

The existence of symmetric orbits is helpful for several reasons. It allows classification of orbits by symmetry properties. Furthermore symmetric orbits have points on the fixed planes of the symmetry; this reduces the numerical computations needed to find the orbits. Symmetric periodic orbits give useful information on the structure of phase space since they form the centers and edges of resonances, and can be used as approximations to quasiperiodic orbits such as the KAM tori.

Orbits which are local minima of the action appear to often be hyperbolic, though counter-examples can be constructed. Equation (31) implies only that the product of $-R_i$ must be positive for a non-degenerate minimum. In the area preserving case, this implies hyperbolicity.

A projection of periodic orbits onto the configuration space (e.g. Fig. 5) shows that as the system becomes more nonlinear (e.g. the potential energy becomes larger), the orbits with index less than N, tend to avoid the symmetry plane on which the -V is maximum. This is the same mechanism which gives rise to the formation of cantori in the area preserving map, so it seems reasonable to speculate that something similar happens here. When an avoided region is formed around the dominant plane, other such regions are formed by iteration. The index N orbit seems to have a single point in the center of each of these regions. The resulting picture, for an incommensurate orbit, would seem to be a set which is connected, but has an infinity of deleted holes. This is not a Cantor set, but probably a Sierpinski carpet.[32] We hope to present evidence for Sierpinski carpets in a later paper.

A cross section of the phase space structure is obtained by plotting the intersection of symmetric periodic orbits with the symmetry plane, Fig. 11. This shows that the region around a periodic orbit is avoided by orbits with different frequencies. We interpret this region as the cross section of a resonance. Orbits in a resonance can remain trapped for long periods, and while they are trapped have the same frequency as the resonance. Collections of resonances which obey a commensurability relation, $\omega \cdot j = 0$, form channels on the symmetry plane. Chaotic motion appears to take place along the edges of these channels. The collection of channels gives the Arnold web. A description of Arnold diffusion in terms of transistions from one resonance to another would require a better understanding of the resonance boundaries, and a definition for escaping flux like that for area preserving mappings.[9,31]

Acknowledgments

We would like to thank R.S. MacKay for many helpful suggestions, such as the idea of constructing Fig. 11. We gratefully acknowledge useful discussions with S. Kim on rational approximants, R. Helleman and J.M. Mao on bifurcations, J.N. Mather and V. Bangert on existence of minimizing orbits, and I.C. Percival on everything. We learned at Dynamics Days Houston 1988 that S.Y. Kim, and M. Muldoon and A. Katok are carrying out similar calculations and would like to thank them for sharing their insights and results.

R.S. MacKay and D. Rand at the Mathematics Institute of Warwick University organized a great workshop where some of this work was carried out. Support was received from a NATO for international collaboration in research, the UK Science and Engineering Research Council, and U.S. Department of Energy Grant #DE-FG05-80ET-53088.

Appendix A: Constant Twist Case

Lemma: A mapping with constant twist and zero net flux has a generating function

$$F = \frac{1}{2}(q'-q)\cdot b\cdot(q'-q) - V(q) \tag{A1}$$

where b is a symmetric matrix, and $\mathcal{V}$ and $\mathcal{U}$ are periodic functions.

Proof: If the twist is constant then the generating function can be written as

$$F = \frac{1}{2}\left[-q\cdot B\cdot q' + f(q) + g(q')\right]$$

where B is a constant matrix and f and g are arbitrary functions. Periodicity of the mapping implies that the net flux, $\mathcal{F}_m = F(q+m,q'+m) - F(q,q')$ is independent of q and q' for all integer vectors m, or

$$\mathcal{F}_m = f(q+m)-f(q) + g(q'+m)-g(q') - q\cdot B\cdot m - m\cdot B\cdot q' - m\cdot B\cdot m \tag{A2}$$

This implies that f and g can have arbitrary periodic parts, call them $\mathcal{V}$ and $\mathcal{U}$ respectively, and that the remainder must be at most quadratic, thus

$$f(q) = \mathcal{V}(q) + q\cdot C\cdot q + q\cdot D\ ,$$
$$g(q') = \mathcal{U}(q') + q'\cdot E\cdot q' + q'\cdot F$$

for matrices C and E and vectors D and F. Substitution into (A2) implies that $B = C + C^t = E + E^t$, and that $m\cdot(D+F) = \mathcal{F}_m$. Therefore for a solution to exist, the matrix B must be symmetric. Furthermore, if the net flux is zero, $D+F = 0$, and the generating function takes the form

$$F = \frac{1}{2}\left[(q'-q)\cdot B\cdot(q'-q) + (q-q')\cdot D - \mathcal{V}(q) - \mathcal{U}(q')\right] \tag{A3}$$

Equation (A3) can be simplified by the canonical coordinate change $\overline{q} = q$, $\overline{p} = p + {}^1/_2 D + {}^1/_2\nabla\mathcal{U}(q)$ which gives Eq. (A1) in the new coordinates, with $V(q) \equiv {}^1/_2[\mathcal{V}(q) + \mathcal{U}(q)]$. ■

Appendix B: Existence of Periodic Orbits

The existence of a miminum for the periodic action W_ω is guaranteed by the following[11]

Lemma: Let $F(q,q')$ have zero net flux and suppose F_{12} is uniformly negative definite, i.e. $\exists\ B>0$ such that $\mathbf{x}\cdot F_{12}(q,q')\cdot\mathbf{x} \leq -B|\mathbf{x}|^2$. Then $\exists\ \alpha$, and positive β and γ such that

$$F(q,q') \geq \alpha - \beta|q-q'| + \gamma|q-q'|^2 \qquad (B1)$$

Proof:

$$F(q,q') = F(q,q) + \int_0^1 d\lambda F_2(q,\xi_\lambda)\cdot(q'-q)$$

where $\xi_\lambda = (1-\lambda)q + \lambda q'$. Similarly applying this to F_2 yields

$$F(q,q') = F(q,q) + \int_0^1 d\lambda F_2(\xi_\lambda,\xi_\lambda)\cdot(q'-q) - \int_0^1 d\lambda \int_0^\lambda d\mu\ (q'-q)\cdot F_{12}(\xi_\mu,\xi_\lambda)\cdot(q'-q)$$

$$\geq \alpha - \beta|q'-q| + \gamma|q'-q|^2$$

where $\alpha = \min F(q,q)$ and $\beta = \max|F_2(q,q)|$ exist since $F(q,q)$ is periodic for zero net flux, and $\gamma = {}^1/_2 B$. ■

Corollary 1: There exists a minimum of W_ω for each $\omega = (m,n)$.

Proof: Equation (B1) implies that F has a lower bound, thus W_ω does as well. Furthermore, the set $\{q,q' \mid q\in\mathcal{T}^N,\ q'\in\mathcal{R}^N,\ F(q,q') \leq C\}$ is compact since (B1) implies that F<C corresponds to bounded $|q-q'|$. Similarly the set

$$S = \left\{ q_0,q_1,\ldots q_{n-1} \,\middle|\, q_0\in\mathcal{T}^N,\ (q_1,\ldots q_{n-1})\in\mathcal{R}^{(n-1)N},\ W_\omega(q_0,q_1,\ldots q_{n-1}) < C' \right\}$$

is compact. W_ω is continuous and bounded on $\mathcal{S}$, thus a minimum exists. ■

Corollary 2: There exist at least N+1 (and generically at least 2^N) periodic orbits for each $\omega = (m,n)$.

Proof: Consider the constrained minimization of W_ω for fixed q_0. Such a minimum exists by virtue of the preceding considerations. Define the function

$$F(q_0) \equiv \min_{q_1,q_2,\ldots q_{n-1}} W_\omega(q_0,q_1,\ldots q_{n-1})$$

to be this mininum. Of course a critical point of W_ω for fixed q_0 gives an orbit segement, but not generally a periodic orbit. However, zero net flux implies F is a function on $\mathcal{T}^N$; such a function has at least N+1 critical points. In fact, Morse theory[23] implies that if the critical points are non-degenerate, there must be at least 2^N; furthermore, non-degeneracy is generic. In this case there are at least N!/i!(N-i)! orbits with index i. Each critical point of F gives a periodic orbit. ■

Corollary 3: There exist at least 2^N symmetric periodic orbits for each $\omega = (m, n)$, one for each symmetry class.

Proof: Consider the minumum of the half orbit action:

$$W_k(q_1,q_2,\ldots,q_{k-1}) \equiv W(q_0,q_1,\ldots,q_{k-1},q_k)\Big|_{\substack{q_0\in Fix(S)\\ q_k\in Fix(S')}}$$

where S and S' are two symmetry planes and S' is SR_m or TSR_m for n even or odd, respectively, according to Eq. (28). Critical points of W_k give a periodic orbit of period n by using Eq. (28) with i=0 to define the z_j for $j\in[k+1,n]$. Such critical points exist because W_k is bounded from below and the set $W_k \leq C$ is compact. ■

The symmetric periodic orbits of Corollary 3 do not necessarily coincide with the orbits of Corollary 2.

Appendix C: Numerical Techniques

Finding an orbit for given frequency and parameters is equivalent to solving a system of nonlinear equations. By definition, a periodic orbit of frequency (m,n) is obtained by finding a point z_0 such that its n-th iterate is $R_{-m}z_0$, where R is the translation operator defined in Eq. (12). Namely, the system to be solved is $f(z_0) \equiv R_m T^n z_0 - z_0 = 0$, where T is the map. This requires a 2N-dimensonal root finder for the 2N dimensonal mapping. However, as will be shown below, it is possible to reduce the search to N dimensions, providing we consider only symmetric orbits. Note that the evaluation of the $f(z_0)$ involves iterating the map n times, the period of the orbit. Alternatively, one can search for stationary configurations of the action function according to the variational principle presented in §2. In this case the set of equations to be solved is $f(q_0, q_2, \ldots, q_{n-1}) \equiv \nabla W_\omega = 0$, where W_ω is the action. This involves solving a system of N × n nonlinear simultaneous equations.

For the fixed point and period two orbits, either system of equations can be solved analytically as shown in §3. For longer orbits, i.e. the typical case, one must rely on numerical computations. There are many methods in the literature for iterative solution of a set of nonlinear equations. One of them, Broyden's method, has been used to find most of the periodic orbits in our present work. However, we do not claim that this method is the optimal choice to our problem. In general, for iterative algorithms of this kind, there is no sufficient test for existence of solutions. Convergence of an algorithm to a solution is guaranteed only when the solution exists and the initial trial solution is within the basin of attraction for the desired solution.[33] This basin typically has a very complicated structure; however, if the trial solution is chosen sufficiently close to the actual solution, this algorithm has been shown to exhibit excellent convergence.

In our case, the orbits are known to exist. However, the equations are so complicated that it is hopeless to analyze the behavior of the function in the neighborhood of a solution. Thus the best procedure is to try several methods to find the most suitable one to our particular problem.

Broyden's method,[34] is a quasi-Newton or variable metric method. Briefly, the algorithm is

problem: Solve $f(x^*)=0$

Define $f_k=f(x_k)$, $s_k=x_k-x_{k-1}$ and $y_k=f_k-f_{k-1}$

Input: x_o, B_o

Do loop for k from k=1

$$s_k = - B_{k-1}^{-1} \cdot f_{k-1} \qquad (C1)$$

$$B_k = B_{k-1} + \frac{f_k s_k^t}{|s_k|^2} \quad \text{or} \quad B_k^{-1} = B_{k-1}^{-1} - \frac{B_{k-1}^{-1} f_k s_k^t B_{k-1}^{-1}}{s_k^t B_{k-1}^{-1} y_k} \qquad (C2)$$

Continue until $|s_k| <$ given tolerance

Here the vector s_k is the correction to the approximate root x_k and the matrix B_k is an approximation of the exact Jacobian at x_k.

It has been shown that this algorithm converges superlinearly to the solution x^*, if a converging sequence $\{x_k\}$ exists.[35] That is,

$$\lim_{k\to\infty} \frac{|x_{k+1} - x^*|}{|x_k - x^*|} = 0$$

The B_k's are uniquely determined by the following two conditions:

$$B_k \cdot s_k = y_k \qquad (C3)$$

$$B_k \cdot z = B_{k-1} \cdot z \quad \text{for any } z \text{ such that } s_k \cdot z = 0 \qquad (C4)$$

Equation (C3) implies that B_k is an approximate Jacobian at x_k. For the one dimensional case, the approximate Jacobian corresponds to using the secant line to determine s_k at each stage. For the multi-dimensional case the first condition does not uniquely determine B_k. There are various ways to fix B_k; for Broyden's method the approximate Jacobian is determined using Eq. (C4). This condition together with Eq. (C3) uniquely fixes B_k. The resulting B_k's satisfy the recursion formula (C2). This recursive relation offers significant reduction in the work involved in the calculation of the Jacobian, which usually requires $o(n^2)$ function evaluations at each stage. There are also several alternatives to (C4) which give a symmetric B_k.[36] In our case, we observe that the latter methods involve more computations and do not give any improvement in convergence.

We employ Broyden's method to find periodic orbits by solving $f(z_o) \equiv R_m T^n z_o - z_o = 0$. As mentioned above, the required four dimensional search for z_o can be reduced to a two dimensional one for symmetric periodic orbits. This is done by utilizing the properties of the symmetric orbits discussed in §4. For a given frequency, the symmetry plane of z_o determines the symmetry plane of z_k by Eq. (28). Choose a symmetry plane of z_o and let p_o be, say, the momentum of a point z_o on the plane. The function f depends only on p_o i.e., $f = f(p_o)$. Its value is determined by the equations for the symmetry plane of z_k; for example, $f = q_k - {}^1/_2 m$ for z_k on $\mathrm{Fix}(SR_m)$ or $f = p_k - 2q_k + m$ for z_k on $\mathrm{Fix}(TSR_m)$ (See Eq.(26)). Therefore the function f is a two dimensional vector. The explicit form of f varies depending on the frequencies and the symmetry plane of z_o as shown in Table 1. All cases can be neatly combined into one formula as follows.

$$f(p_o) = p_k - C \cdot (m + R - 2q_{k-1}) \qquad (C5)$$

where $C = {}^1/_{OE} \, {}^{-TS \cdot OE}/_2$. Here OE=1 for odd n and OE=2 for even n, and TS=1 when z_o is on the symmetry plane of TS symmetry family (TS, $TSR_{(0,1)}$, etc.) and TS=0 otherwise. R represents the translation of the symmetry plane of z_o , i.e., R=(1,0) for $SR_{(1,0)}$ or $TSR_{(1,0)}$, R=(0,1) for $SR_{(0,1)}$ or $TSR_{(0,1)}$ and etc. Finally the other half of the orbit is obtained by using the symmetry relation (27). Numerically this method

can converge to the half orbit for cases when iteration of $\mathbf{z}_k$ fails to converge to the second half of the orbit.

Choosing a good initial trial, $\mathbf{p}_o$, is critical for the performance of any iterative solution technique. In the small parameter range, we choose $\mathbf{p}_o = {}^m/_n$, i.e., the rotation number of the orbit. This works well as long as the orbit is not far from the uniform rotation configuration. For an orbit in a large parameter, $\mathbf{p}_o$ can be chosen by extrapolating the orbits obtained in smaller parameters. We use the identity matrix for $\mathbf{B}_o$. Using a Jacobian for $\mathbf{B}_o$ usually does not give any improvement in convergence. The recursion relation for $\mathbf{B}_k$ rather than for its inverse (see Eq. (C2)) is used because the former involves less computations and the step (C1) can be easily done for a 2×2 matrix $\mathbf{B}_k$.

The mapping iteration scheme becomes impractical for a strongly unstable orbit because upon iterations of the map an initial numerical error grows exponentially. However, as long as the magnitude of the smallest multiplier is sufficiently large compared to the computer precision, this scheme works and is the simplest to implement.

References

1. J. Wisdom, "The origin of the Kirkwood gaps: a mapping for asteroidal motion near the 3/1 commensurability," Astron J. **87**, 577 (1982).

2. A.J. Dragt, "Lectures on nonlinear orbit dynamics," AIP Conf. Proc. **87** (1982); in Nonlinear Dynamics and the Beam-Beam Interaction, Brookhaven, 1979, AIP Conf. Proc #57, M.Month and J.Herrera (eds.), p. 236 (AIP, New York, 1979).

3. A.J. Lichtenberg and M.A. Lieberman, Regular and Stochastic Motion (Springer-Verlag, New York,1983); J.E.Howard, A.J. Lichtenberg, M.A. Lieberman, and R.H. Cohen, "Four-dimensional mapping model for two-frequency electron cyclotron resonance heating," Physica **20D**, 259(1986).

4. V.I. Arnold, Mathematical Methods of Classical Mechanics, (Springer-Verlag, New York, 1978).

5. R. Broucke, "Stability of periodic orbits in the elliptic three-body problem," AIAA Journal **7**, 1003 (1969); E. Davoust and R. Broucke, "A manifold of periodic orbits in the planar general three-body problem with equal masses," Astron. Astrophys. **112**, 305(1982).

6. J.N. Mather, "Existence of quasi-periodic orbits for twist homeomorphisms of the annulus," Topology **21**, 457(1982).

7. S. Aubry, "The twist map, the extended Frenkel-Kontorova model and devil's staircase," Physica **7D**, 240 (1983); S. Aubry and P.Y. Le Daeron, "The discrete Frenkel-Kontorova model and its extensions," Physica **8D**, 381 (1983).

8. J.M. Greene, "A method for determining a stochastic transition," J. Math. Phys. **20**, 1183 (1979); R.S. MacKay, "A renormalisation approach to invariant circles in area-preserving maps," Physica **7D**, 283 (1983).

9. R.S. MacKay, J.D. Meiss, and I.C. Percival, "Stochasticity and transport in Hamiltonian systems," Phys. Rev. Lett. **52**, 697(1984); "Transport in Hamiltonian systems," Physica **13D**, 55(1984).

10. D. Bernstein and A. Katok, "Birkhoff periodic orbits for small perturbations of completely integrable Hamiltonian systems with convex Hamiltonians," Invent. math. **88**, 225 (1987).

11. R.S. MacKay, J.D. Meiss, and J. Stark, "Converse KAM theory for symplectic twist maps," University of Warwick preprint(1988).

12. Q. Chen, R.S. MacKay, and J.D. Meiss, "Existence of cantori for symplectic maps in more than two dimensions," in preparation (1988).

13. C. Froeschle, "On the number of isolating integrals in systems with three degrees of freedom," Astrophys. Space Sci. **14**, 110 (1971); C. Froeschle, "Numerical study of a four-dimensional mapping," Astron. Astrophys.**16**, 172 (1972); C. Froeschle and J.-P. Scheideker, "Numerical study of a four-dimensional mapping. II" Astron. Astrophys. **22**, 431 (1973).

14. B.V. Chirikov, "A universal instability of many-dimensional oscillator systems," Phys. Rep. **52**, 265 (1979).

15. J.M. Mao, I.I. Satija, and Bambi Hu, "Period doubling in four-dimensional symplectic maps," Phys. Rev. **A34**, 4325 (1986); J.M. Mao and R.H.G. Helleman, "New Feigenbaum constants for four-dimensional volume-preserving symmetric maps," Phys. Rev. **A35**, 1847(1987); J.M. Mao and R.H.G. Helleman, "Non-symmetric four-dimensional volume-preserving maps: Universality classes of period doubling," Phys. Rev. **A37**, 3475 (1987);

16. J. Moser, "New aspects in the theory of stability of Hamiltonian systems," Comm. pure and applied Math., vol**XI**, 81(1958).

17. J.E. Howard and R.S. MacKay, "Linear stability of symplectic maps," J. Math. Phys. **28**, 1036(1987).

18. R. Abraham and J. Marsden, Foundations of Mechanics, (Benjamin/Cummings, Reading, 1978), p. 308; R. DeVogelaere, in Contributions to the Theory of Nonlinear Oscillations, (Princeton Univ. Press, Princeton,1958), S. Lefschetz (ed), vol IV, p. 53.

19. R.S. MacKay, "Renormalisation in area preserving maps", Ph.D. Thesis, (Univ. Microfilms, Ann Arbor, 1982).

20. This result is a consequence of the symplectic Bochner Theorem proved by V.L. Ginzburg and M.B. Sevryuk in a letter to R.S. MacKay dated Jan. 18, 1988.

21. R. Rimmer, "Symmetry and bifurcation of fixed points of area preserving maps," Journal of Diff. Eq. **29**, 329 (1978).

22. G.A. Hedlund, "Geodesics on a two-dimensional Riemannian manifold with periodic coefficients," Ann. Math. **33**, 719(1932)

23. J. Milnor, Morse Theory, Annals of Mathematical Studies **51**, (Princeton Univ. Press, 1963).

24. R.S. MacKay and J.D. Meiss, "Linear stability of periodic orbits in Lagrangian systems," Phys. Lett. **98A**, 92 (1983).

25. A.Y. Khinchin, Continued Fractions (Univ. of Chicago Press, Chicago, 1964).

26. S. Kim and S. Ostlund, "Simultaneous rational approximations in the study of dynamical systems," Phys. Rev. **A35** (1987).

27. L. Bernstein, The Jacobi-Perron Algorithm: Its Theory and Application (Springer-Verlag, Heidelberg, 1971).

28. A.J. Brentjes, Multidimensional Continued Fraction Algorithms (Mathematisch Centrum, Amsterdam, 1981).

29. G.H. Hardy and E.M. Wright, An Introduction to the Theory of Numbers (Clarendon Press, Oxford, 1954).

30. K. Kaneko and R.J. Bagley, "Arnold diffusion, ergodicity and intermittency in a coupled standard mapping," Phys. Lett. **110A**, 435 (1985).

31. R.S. MacKay, J.D. Meiss and I.C. Percival, "Resonances in area-preserving maps," Physica **27D**, 1(1987).

32. W. Sierpinski, "Sur une courbe cantorienne qui contient une image biunivoque et continue de toute courbe donnee," Compte Rendus Acad. Sci. Paris **162**, 629 (1916).

33. For definitions and general arguments on the convergence rate of iterative algorithms, see J.M. Ortega and W.C. Rheinboldt, Iterative solution of nonlinear equations in several variables, (Academic Press, New York, 1970).

34. C.G. Broyden, "A class of methods for solving nonlinear simultaneous equations," Math. Comp. **19**, 577 (1965).

35. C.G. Broyden, J.E. Dennis Jr. and J.J. More, "On the local and superlinear convervence of Quasi-Newton methods," J. Inst. Math. Appl. **12**, 223 (1973).

36. J.E. Dennis Jr. and J.J. More, "Quasi-Newton methods, motivation and theory," SIAM Review **19**, 46 (1977); E. Polak, Computational method in optimization, (Academic Press, New York, 1971).

Table 1

(m_1,m_2,n)	(q_0,p_0)	(q_k, p_k)
(o,o,e)	S $SR_{(1,0)}$ TS $TSR_{(1,0)}$	$SR_{(1,1)}$ $SR_{(0,1)}$ $TSR_{(1,1)}$ $TSR_{(0,1)}$
(e,o,e)	S $SR_{(1,0)}$ TS $TSR_{(1,0)}$	$SR_{(0,1)}$ $SR_{(1,1)}$ $TSR_{(0,1)}$ $TSR_{(1,1)}$
(o,e,e)	S $SR_{(0,1)}$ TS $TSR_{(0,1)}$	$SR_{(1,0)}$ $SR_{(1,1)}$ $TSR_{(1,0)}$ $TSR_{(1,1)}$
(o,o,o)	S $SR_{(1,0)}$ $SR_{(0,1)}$ $SR_{(1,1)}$	$TSR_{(1,1)}$ $TSR_{(0,1)}$ $TSR_{(1,0)}$ TS
(e,o,o)	S $SR_{(1,0)}$ $SR_{(0,1)}$ $SR_{(1,1)}$	$TSR_{(0,1)}$ $TSR_{(1,1)}$ TS $TSR_{(1,0)}$
(o,e,o)	S $SR_{(1,0)}$ $SR_{(0,1)}$ $SR_{(1,1)}$	$TSR_{(1,0)}$ TS $TSR_{(1,1)}$ $TSR_{(0,1)}$
(e,e,o)	S $SR_{(1,0)}$ $SR_{(0,1)}$ $SR_{(1,1)}$	TS $TSR_{(1,0)}$ $TSR_{(0,1)}$ $TSR_{(1,1)}$
(e,e,e)	S $SR_{(1,0)}$ $SR_{(0,1)}$ $SR_{(1,1)}$ TS $TSR_{(1,0)}$ $TSR_{(0,1)}$ $TSR_{(1,1)}$	S $SR_{(1,0)}$ $SR_{(0,1)}$ $SR_{(1,1)}$ TS $TSR_{(1,0)}$ $TSR_{(0,1)}$ $TSR_{(1,1)}$

Table 1 Caption

Symmetry Planes for the four symmetric orbits with frequency (m_1,m_2,n) of a 4D reversible map. There are eight classes of frequencies depending on whether the frequency components are even "e" or odd "o". Each orbit has its first point on the plane in the column (q_0,p_0) and its k^{th} point on the plane in the column (q_k, p_k). Here $k = [(n+1)/2]$.

Figure captions

1) Stability regions in the A-B plane. Stability type for each region is determined by two multiplier pairs whose natures are represented with symbols; $\mathcal{E}$ for elliptic, $\mathcal{H}$ for regular hyperbolic, I for inversion hyperbolic and $\mathcal{CQ}$ for complex quadruplet.

2a) Stability diagram for the fixed point at $p= 0$ and $q= 0$ as a function of k_1 and h for $k_2=0$. Diagrams for the three other fixed points are obtained by flipping this vertically and/or horizontally. No region of complex instability ($\mathcal{CQ}$) occurs. The Krein signature in the region $\mathcal{EE}$ is negative definite.

2b) Stability of the orbit with frequency (1,1,2) on the Fix(S) plane for $k_2=0$. The diagram is symmetric under $k_1 \rightarrow -k_1$. To obtain the corresponding diagram for the orbit on $Fix(SR_{(1,0)})$ let $h \rightarrow -h$. There are three elliptic regions; the Krein signature in the $\mathcal{EE}1$ region is negative definite and in $\mathcal{EE}2$ and $\mathcal{EE}3$ is mixed.

3) Collision of multiplier pairs on complex plane. The multipliers of mixed Krein signatures split off to form a quadruplet after collision. (a) Collision on the unit circle causes the stability to change from $\mathcal{EE}$ to $\mathcal{CQ}$. (b) Collision on the real axis causes a transition from $\mathcal{HH}$ to $\mathcal{CQ}$ for the positive axis and from II to $\mathcal{CQ}$ for the negative axis.

4) Symmetry planes projected onto the canonical p_1-q_1 and p_2-q_2 planes. For example, $Fix(TSR_{(1,0)})$ is projected onto $p_1=2q_1-1$ on

p_1-q_1 plane and $p_2=2q_2$ on p_2-q_2 plane. The symmetric points for the four cases of an orbit with frequency type (e,o,o) are shown. Each orbit intersects two symmetric planes. The orbit on Fix(S) has one point($\mathbf{z}_0$) on Fix(S) and its k^{th} iterate ($\mathbf{z}_k$) on Fix($TSR_{(0,1)}$).

5) Configuration space projection of the four symmetric orbits with frequency (12,21,49) when $k_1=0.4$, $k_2=0.3$, $h=0.65$. Each orbit is represented with symbols; "○" for the orbit on Fix(S), "●" on Fix($SR_{(0,1)}$), "△" on Fix($SR_{(1,0)}$) and "□" on Fix($SR_{(1,1)}$).

6) Sketch of the evolution of the stability of two symmetric orbits with ω = (2,3,4) (a) on the Fix(S) and (b) on the Fix($SR_{(1,0)}$) plane as the parameters vary on the path $k_1=10h$, $k_2=0$. Bifurcations occur each time a stability curve is crossed.

7) Symmetry breaking bifurcations. Bifurcating orbits are of the same frequency as their progenitor. The example shown is for the transition between $\mathcal{EH}$ and $\mathcal{HH}$. (a) direct process. (b) inverse process.

8) Inflection of the action function upon symmetry breaking bifurcation. Here "q" represents one of the configuration coordinates of the orbit, and the dotted line represents the symmetry plane. Prior to bifurcation (a), the orbit is minimizing the action and its index is zero. After the bifurcation (b), the action acquires one convex direction at the extremum point on the symmetry plane. The index of the symmetric orbit becomes one, and the two new minimizing orbits are not symmetric.

9) Kim-Ostlund tree construction. At each level a new vertex is obtained from the Farey sum of vertices of the hypotenuse of the preceding triangle. This gives two new isosceles triangles for which the tree can be continued.

10) Pairs of rationals (ω_1,ω_2) generated by the Kim-Ostlund tree up to level 13. Equivalently, each point represents the intersection point p of a periodic orbit with the frequency $p = (\omega_1,\omega_2)$ on a plane $q=$ constant for the integrable system.

11) Periodic orbits with the frequencies in Fig. 10 for k_1=0.5, k_2=0.3, h=0.2. Higher period orbits are expelled from the vicinity of shorter period orbits creating resonance regions. Furthermore, commensurability lines are expanded into channels which connect the resonances. (a) on $\mathbf{q}$ = (0,0) plane. (b) on $\mathbf{q}$ = ($^1/_2$,$^1/_2$) plane.

12) Sectional view of two stochastic orbits on the $\mathbf{q}$ = 0 plane. Parameters are the same as in Fig. 11. The initial points are $(p_1,p_2,q_1,q_2) = \pm(0.10,0.34,0.0,0.0)$ and the orbit is plotted whenever it falls inside the slice; $-.005 < q_1,q_2 < .005$ up to a time 2×10^8.

13) Projections of one of the irrational tori surrounding resonance zones with frequency (0,0). The initial point, (0.1271, 0.1672, 0.0, 0.0) is selected from one of the stuck points at the edge of the primary resonance in Fig. 12.

14) Staircase of rotation numbers for initial conditions on the line $(p_1,-p_1, 0,0)$. Shown is the frequency ρ_1 versus p_1. An iteration time of 10^3 is used to define $\boldsymbol{\rho}$.

15) Resonance zones for rotation numbers up to level 5 on the Farey tree (where (1,1,2) is level 0). A grid of 200x200 initial conditions is taken on $\mathbf{q}$ = 0 plane. Points are filled in if they give a rotation number in one of the 81 resonances on the tree within a tolerance ε=0.01.

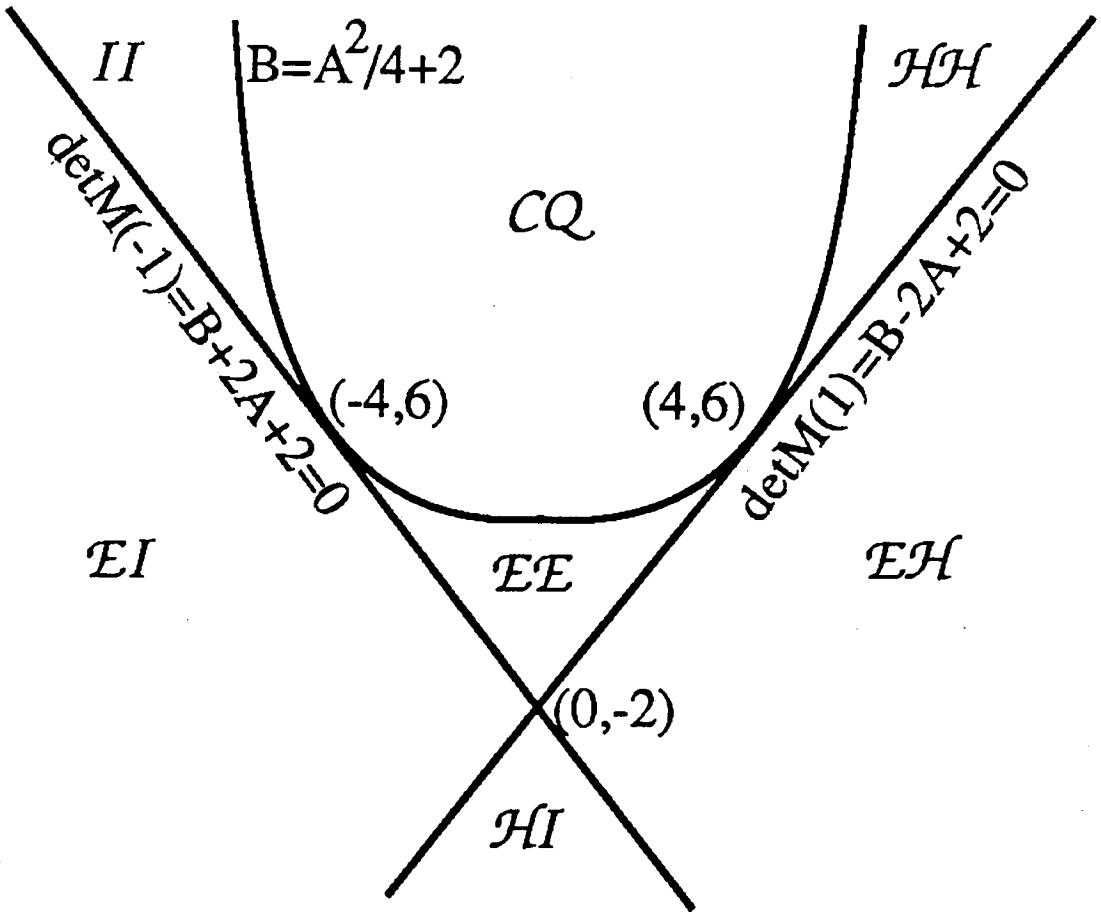

Fig. 1

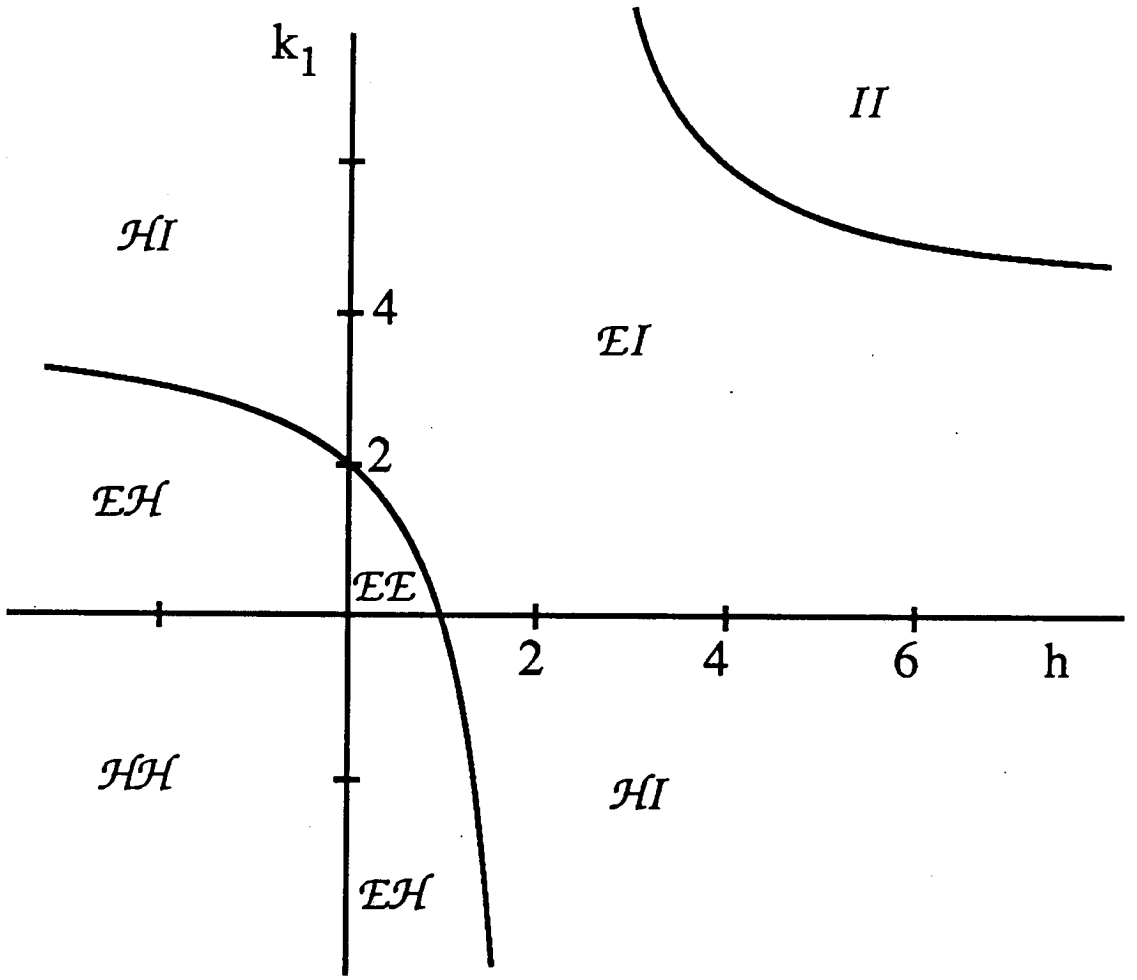

Fig. 2 (a)

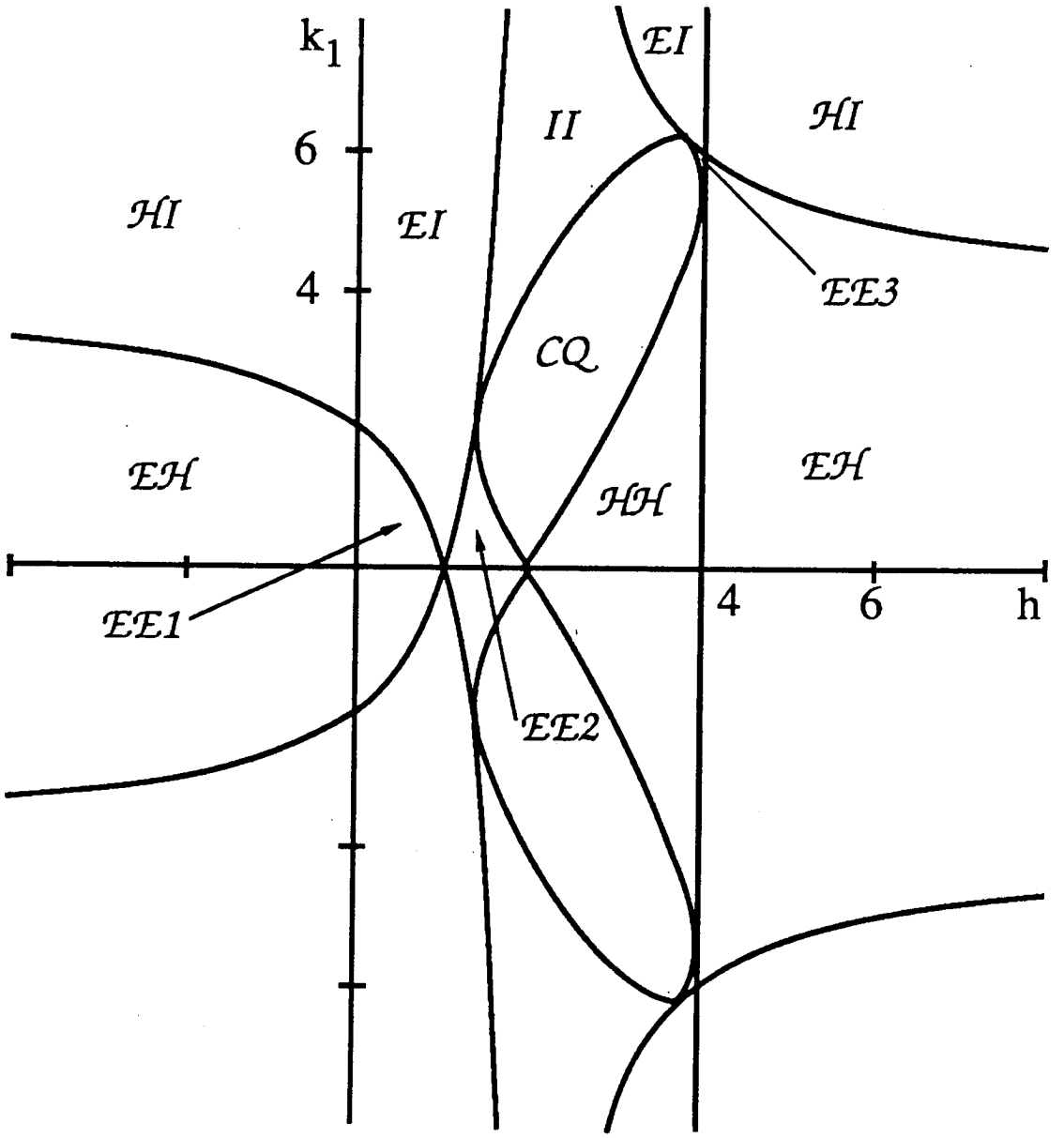

Fig. 2 (b)

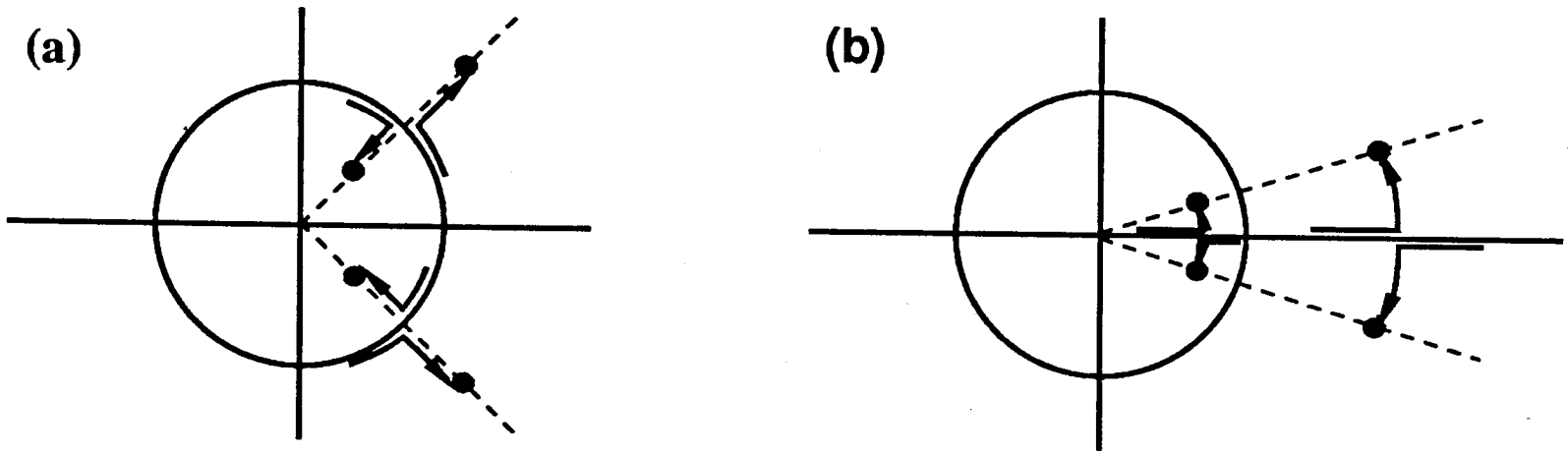

Fig. 3

Z_0	Z_k
S	$TSR_{(0,1)}$
$SR_{(1,0)}$	$TSR_{(1,1)}$
$SR_{(0,1)}$	TS
$SR_{(1,1)}$	$TSR_{(1,0)}$

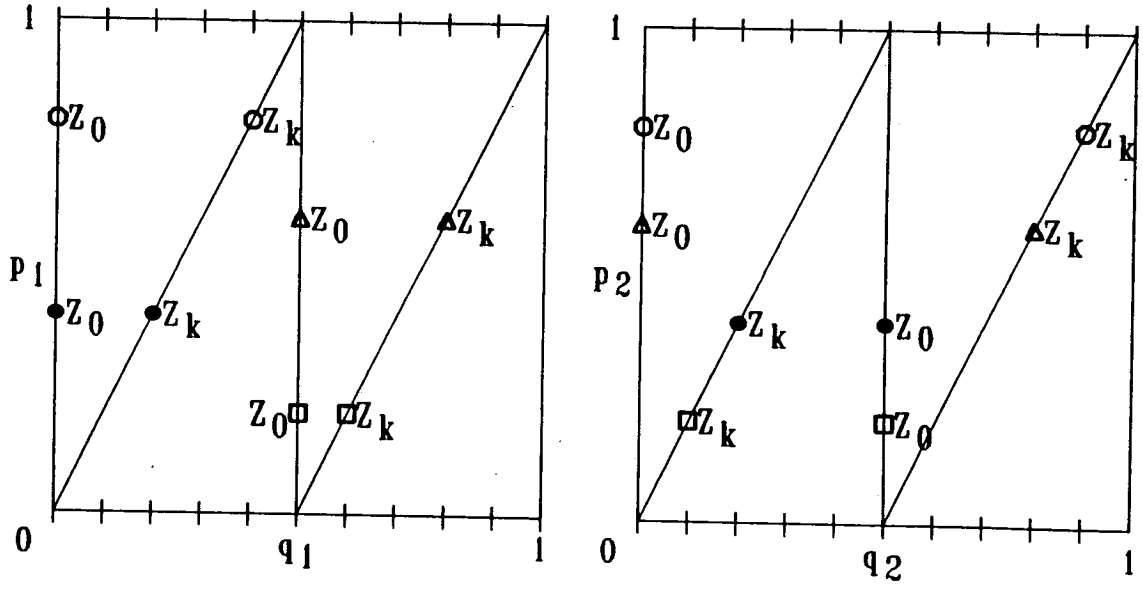

Fig. 4

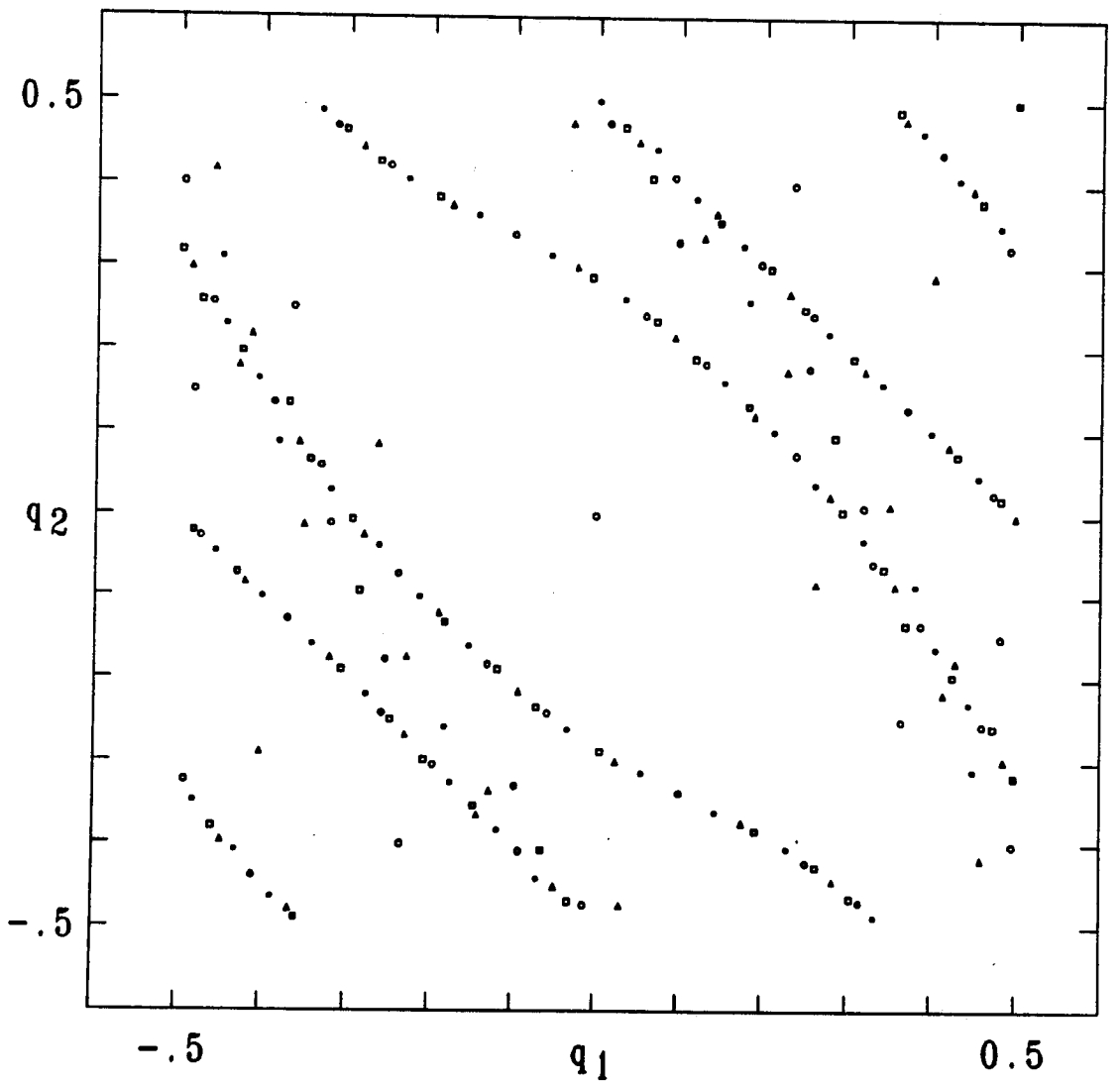

Fig. 5

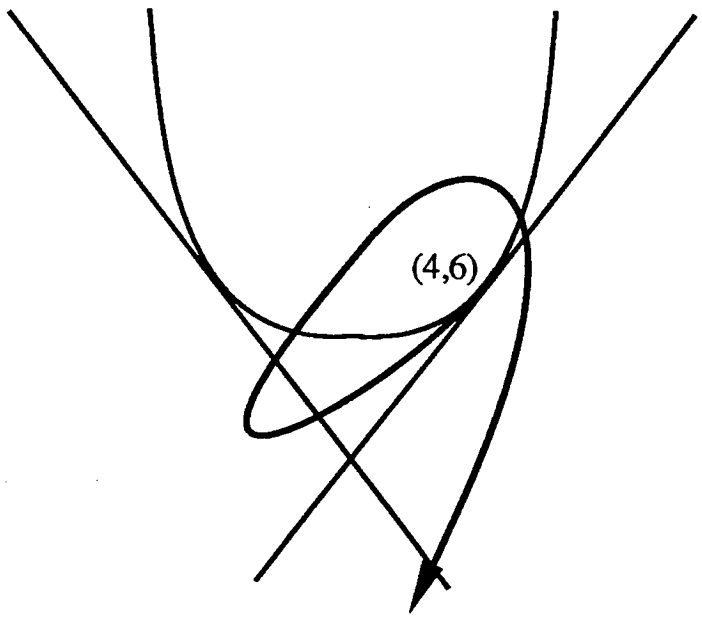

Fig. 6 (a)

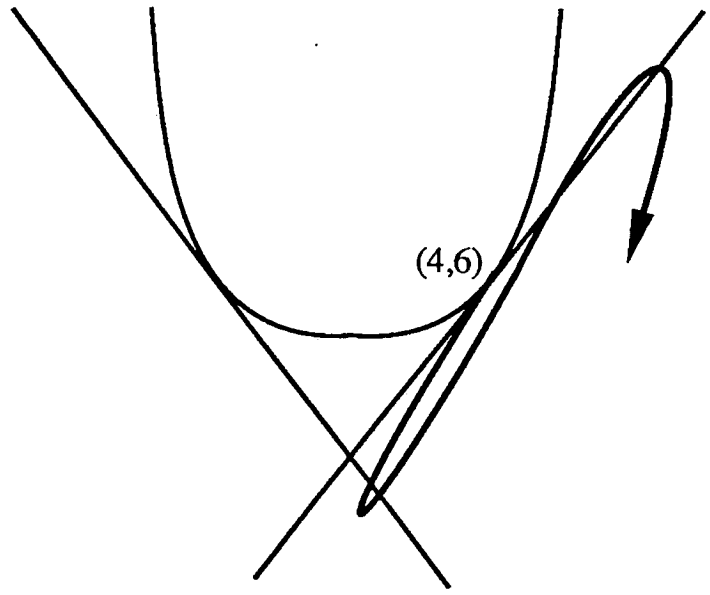

(b)

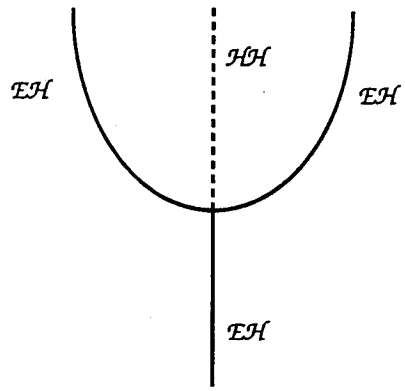

Fig. 7 (a)

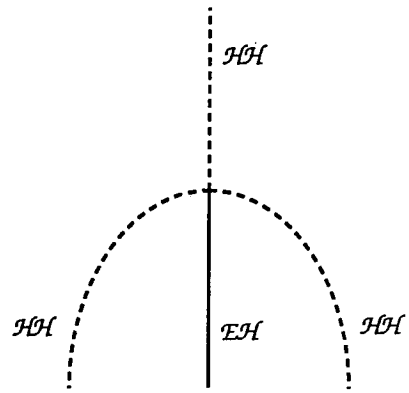

(b)

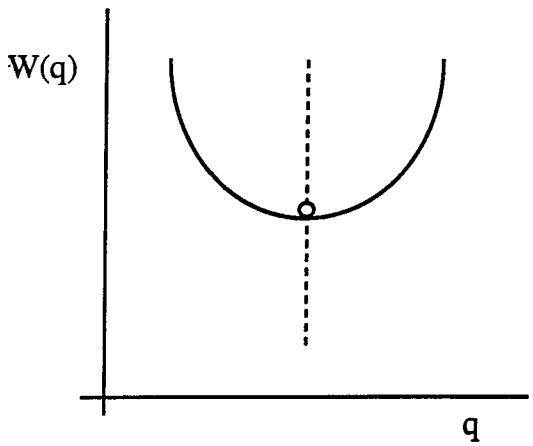

Fig. 8 (a)

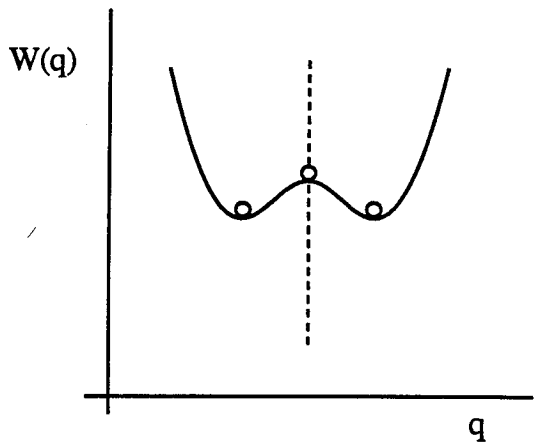

(b)

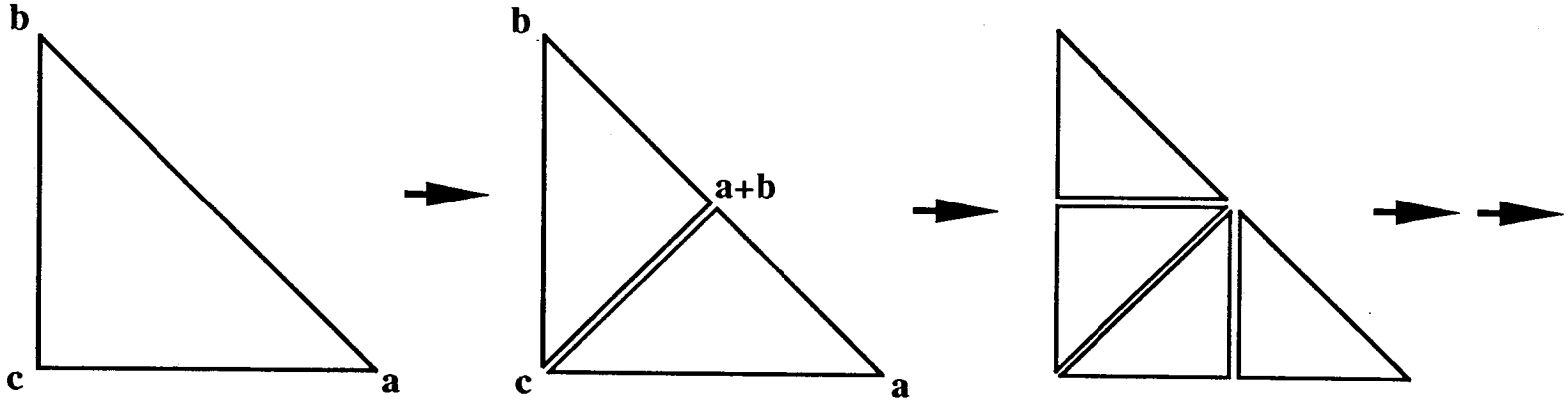

original triangle level 0 level 1

Fig. 9

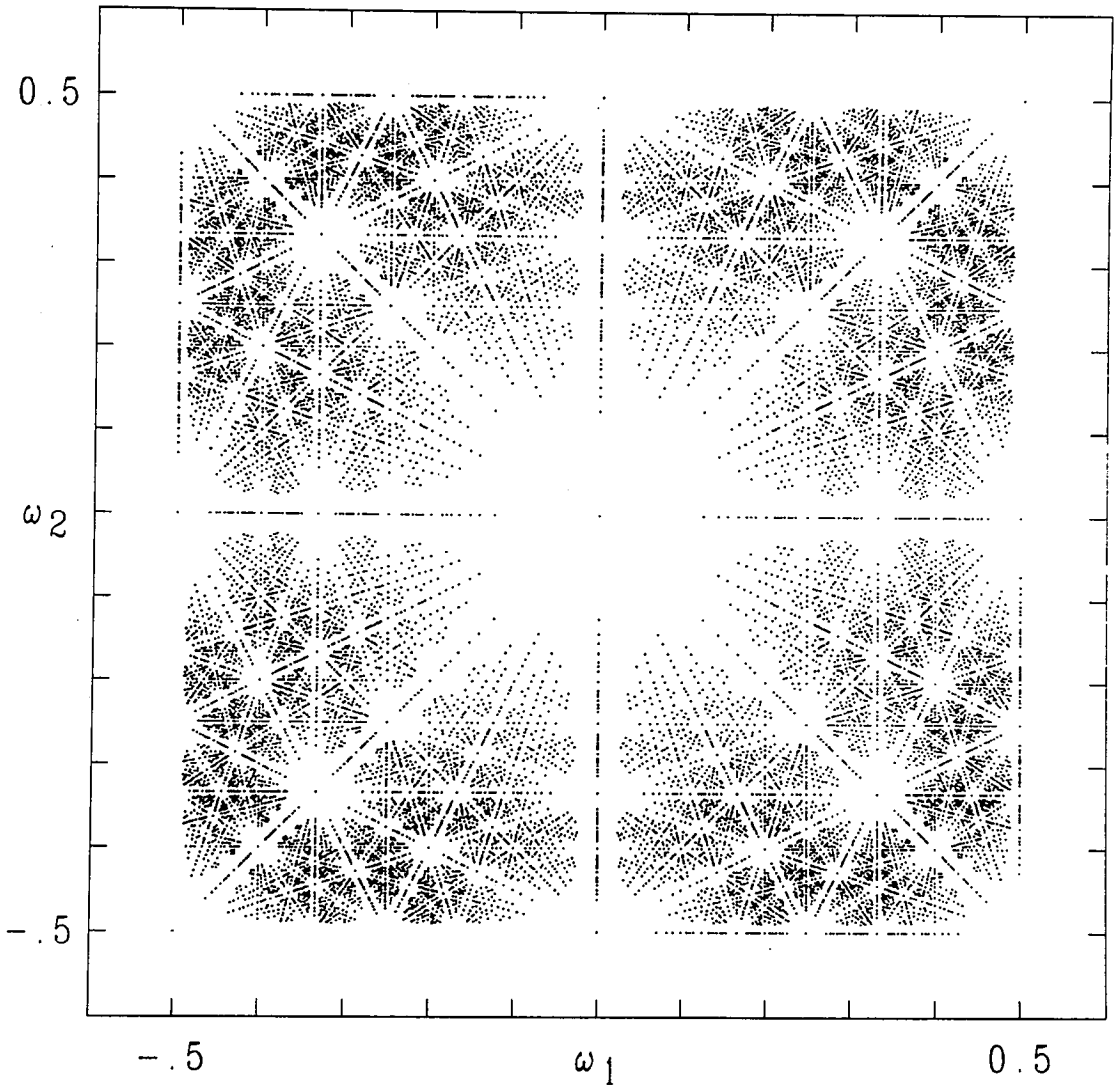

Fig. 10

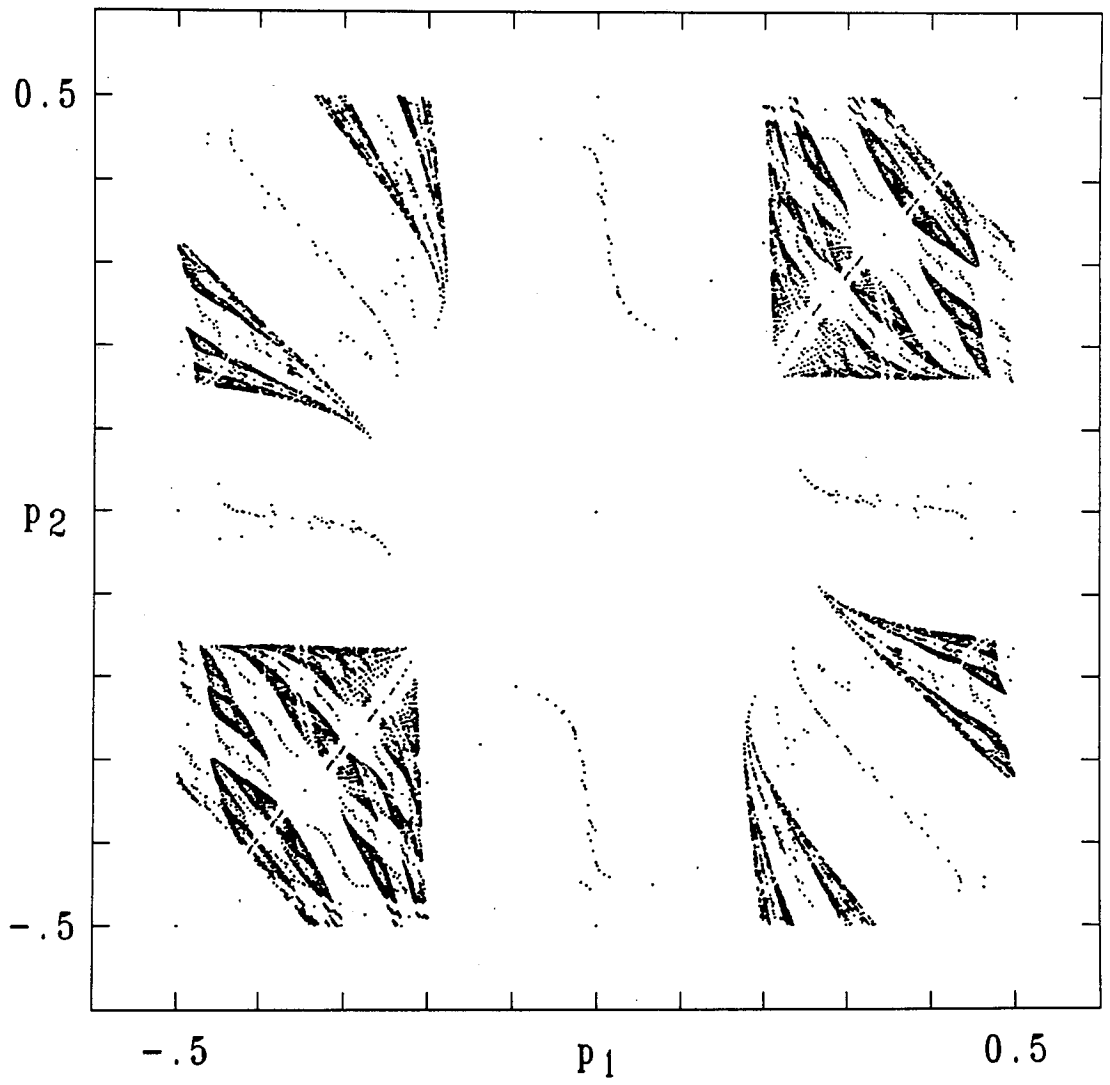

Fig. 11(a)

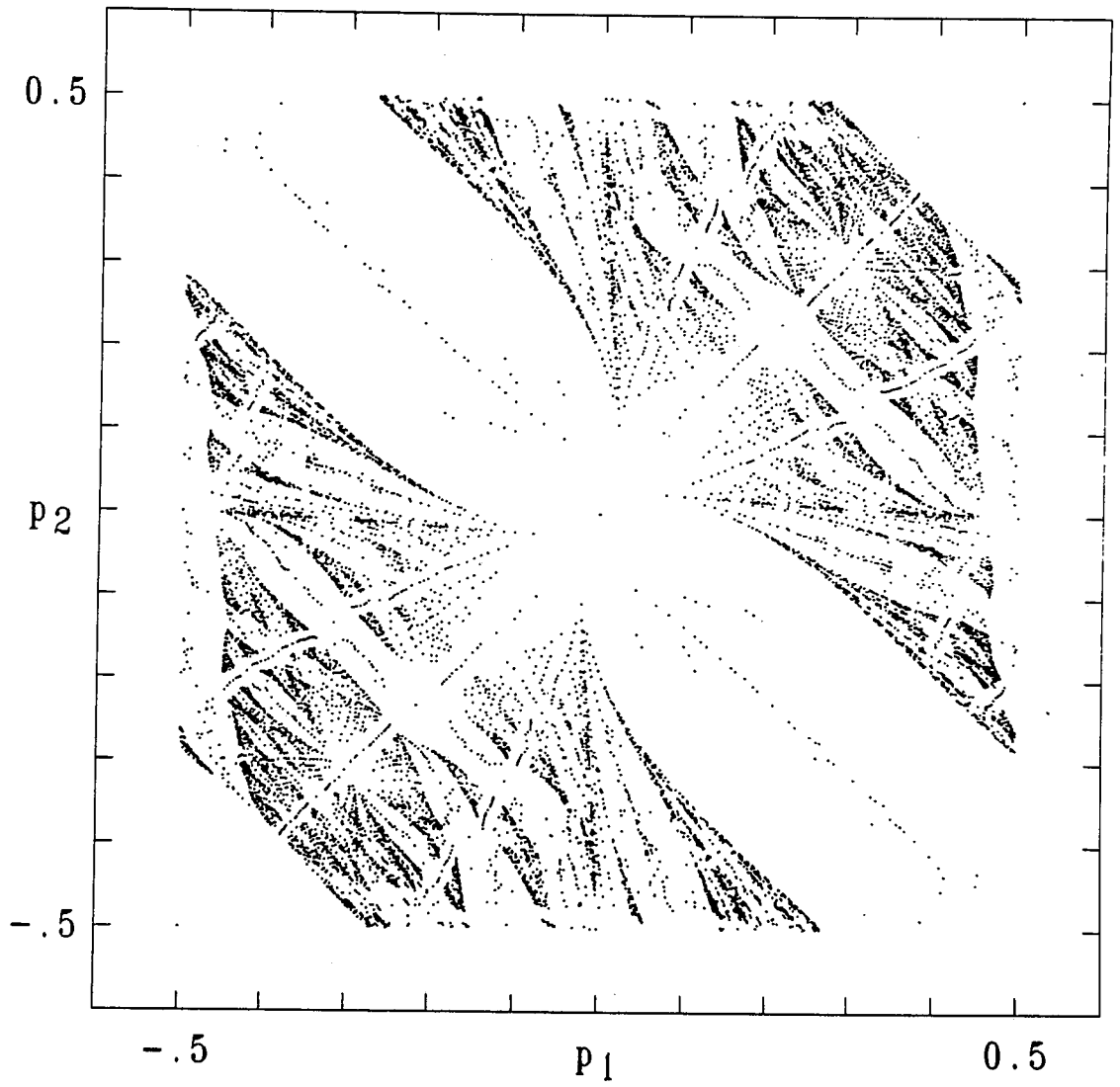

Fig. 11(b)

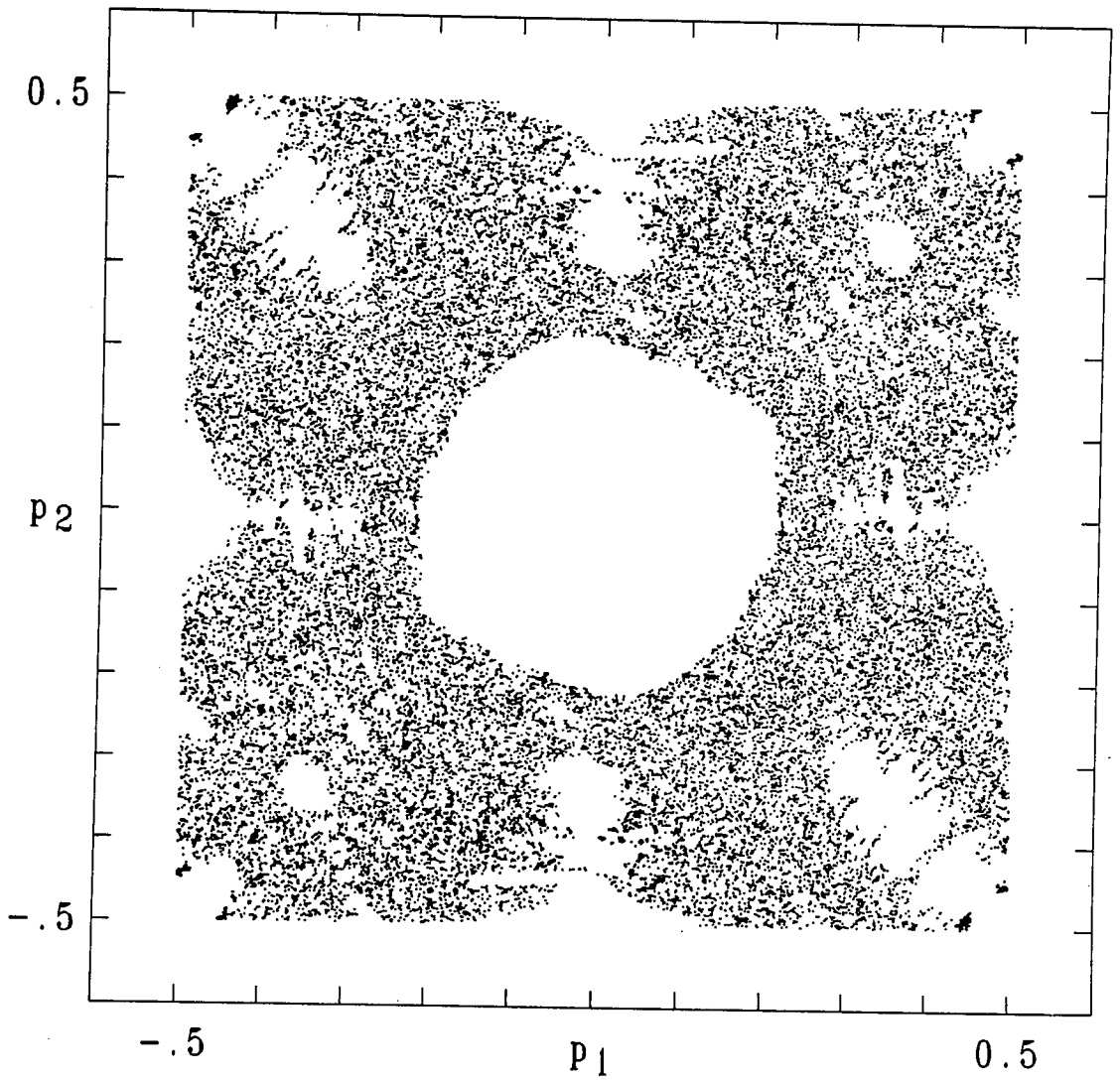

Fig. 12

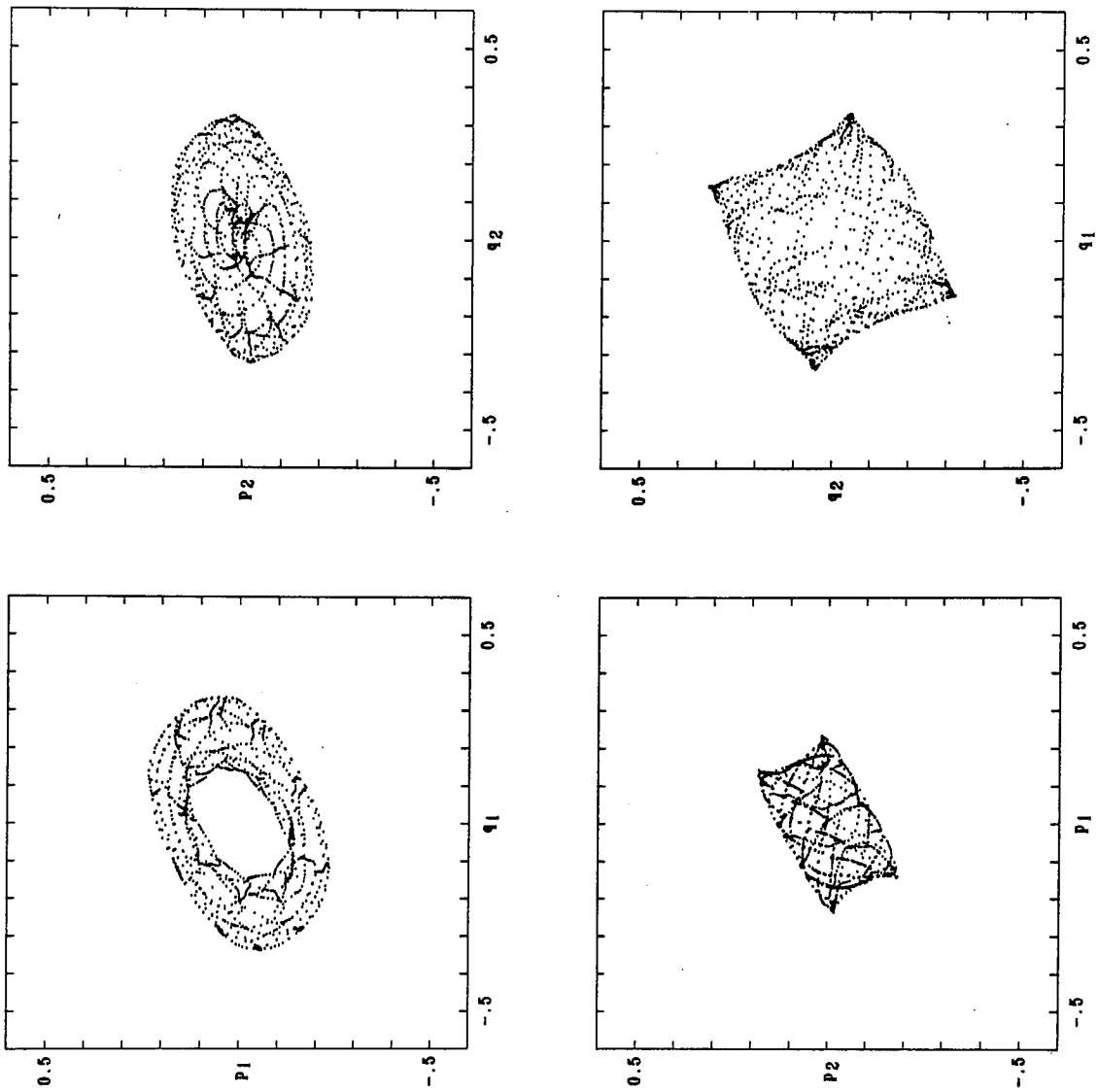

Fig. 13

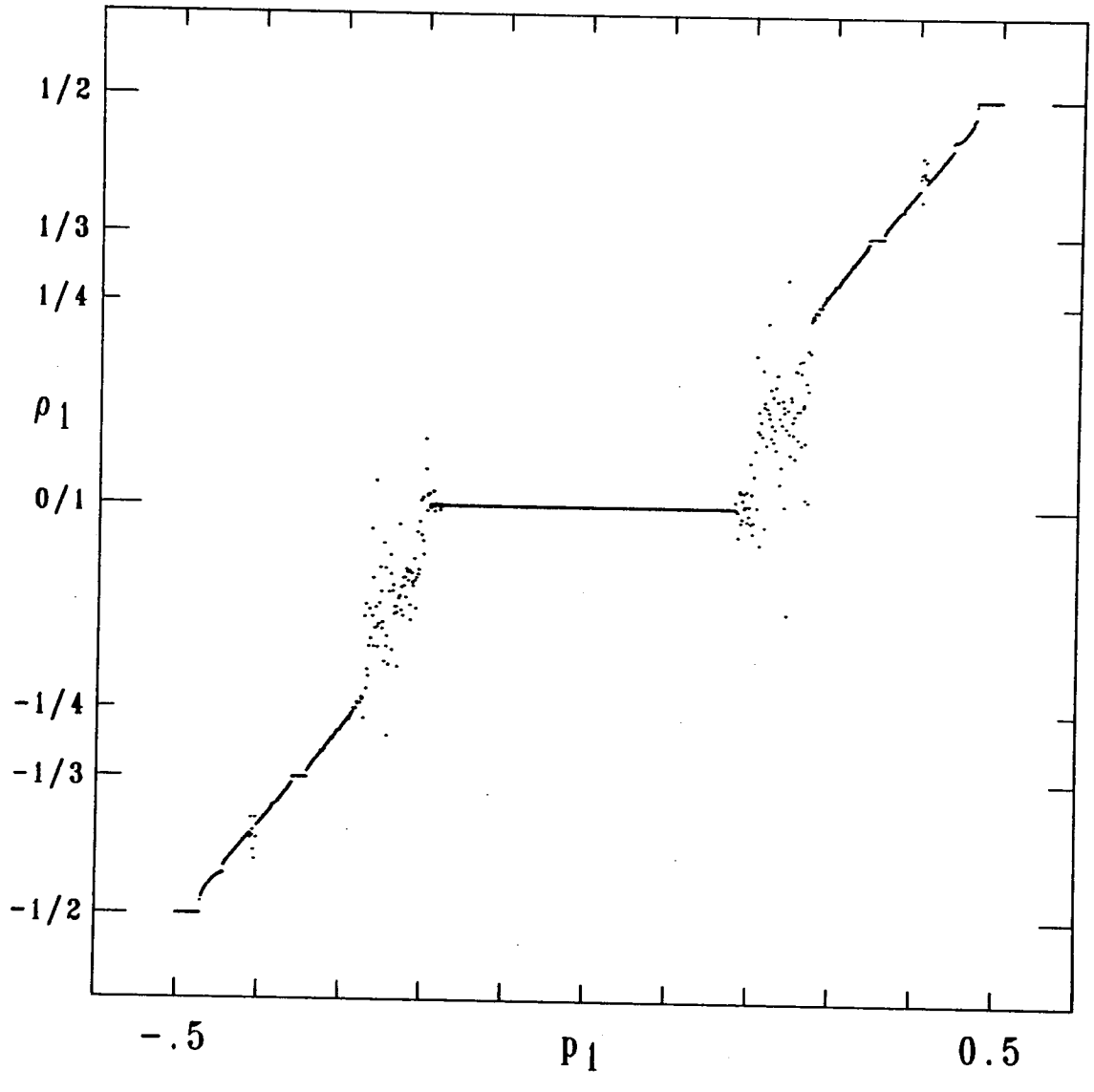

Fig. 14

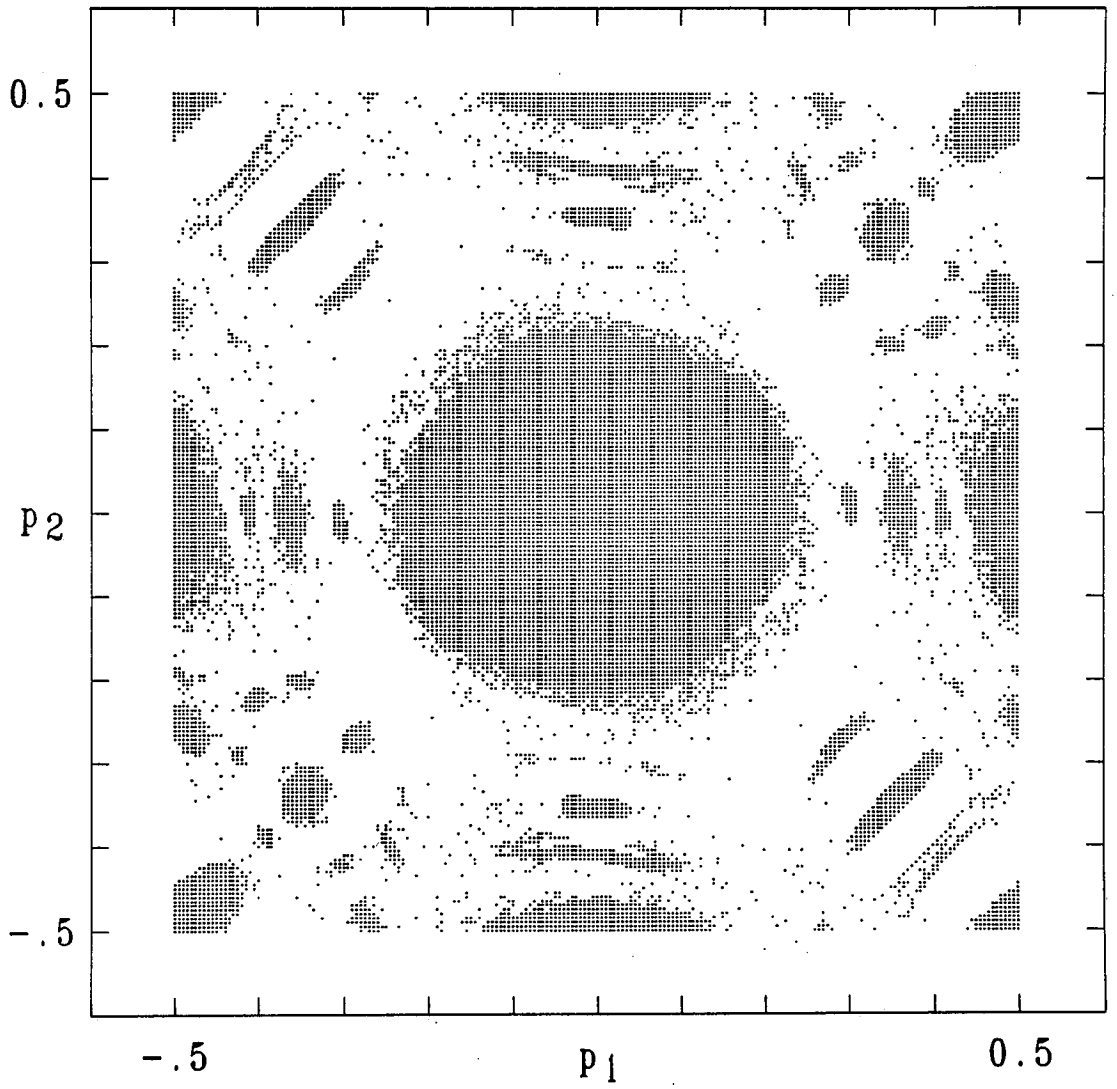

Fig. 15